Electronic Supplementary Material (ESI) for Inorganic Chemistry Frontiers.

ELECTRONIC SUPPLEMENTARY INFORMATION

Biosynthesis of Amino Acid Functionalized Silver Nanoparticles for Potential Catalytic and Oxygen Sensing Applications

Abhishek Chandra[†] and Man Singh[†*]

[†]School of Chemical Sciences, Central University of Gujarat, Gandhinagar-382030, India

Email: mansingh50@hotmail.com, abhishekchandra.15@gmail.com

EXPERIMENTAL SECTION

Estimation of Total Silver Concentration in AgNPs

On completion of the reaction, AgNPs were separated by centrifugation at 17500×g for 20 min. The precipitated AgNPs were collected and digested in aqua regia. The concentration of the Ag^+ ions was measured in triplicate by induced couple plasma-optical emission spectrometer (ICP-OES) (Varian Spectra AA 55, USA) against a standard $AgNO_3$ solution. The concentration of Ag was 1.68 mM in 100 ml aqueous AgNPs dispersion.

Influence of pH, Ionic Strength, Surfactants and Dyes on AgNPs Stability

The colloidal stability of AgNPs at variable pH was studied by recording the UV-visible spectra of 100 μM AgNPs dispersion in the pH range 2–10. The pH of AgNPs dispersion was varied by adding different volumes of 0.1 M aqueous HCl/NaOH. The colloidal stability of AgNPs with increasing ionic strength of the dispersion was studied by recording the UV-visible spectra of 100 μM AgNPs in 0.1 to 2 M aqueous NaCl. The colloidal stability of AgNPs in aqueous surfactants was studied by recording the UV-visible spectra of 30 μM AgNPs in 0.0025 to 0.010 M aqueous cationic surfactant (DTAB), anionic surfactant (SDS), and non-ionic surfactant (OGP). The colloidal stability of AgNPs in aqueous dyes was studied by recording the UV-visible spectra of 30 μM AgNPs dispersion in 10 to 50 μM aqueous cationic dyes (MB) and anionic dye (CR).

For all the colloidal stability experiments, the UV-visible spectra were recorded after 30 min of AgNPs addition to the various aqueous medium. All the experiments were carried out in triplicate.

Catalytic Activity of AgNPs

The AgNPs catalytic activity on MB reduction by acidic $SnCl_2$, while CR and 4-NP reduction by $NaBH_4$ was monitored by UV-visible spectroscopy. For MB reduction, the reactions were carried out in water and in 0.01 M aqueous DTAB/SDS/AOT/T-20. Briefly, in a quartz cuvette, 3ml (0.01 M) aqueous DTAB/SDS/AOT/T-20 was taken and 200 μL (5×10^{-4} M) aqueous MB was added along with 100 μL (0.1M) aqueous $SnCl_2$ (prepared in 1.2 M HC1). To start the catalytic reduction, a fixed volume of the as prepared AgNPs dispersion was added and final volume was made 3.35 mL with Milli-Q water. The final concentration of the AgNPs used in the catalytic MB reduction was 30 μM. The MB color bleaching from blue to colorless was monitored by recording the absorbance at 665 nm. The pH of the reaction solution was ≈ 1.5.

For CR reduction, briefly in a quartz cuvette, 3ml (5×10^{-4} M) aqueous CR was taken and 100 μL (0.2 M) ethanolic $NaBH_4$ was added. To start the catalytic reduction, a known volume of AgNPs dispersion was added and final volume was made 3.2 mL with Milli-Q water, thereby making its final concentration 30 μM. The color bleaching of CR from reddish-orange to colorless was monitored by recording the UV-visible spectra for upto 20 min.

For 4-Nitrophenol reduction, briefly in a quartz cuvette, 3ml (3.5×10^{-4} M) aqueous 4-NP was taken and 100 μL (0.2 M) $NaBH_4$ was added. To start the catalytic reduction, a known volume of AgNPs dispersion was added and final volume was made 3.2 mL with Milli-Q water, thereby making its final concentration 30 μM. The color change of 4-Nitrophenol from bright yellow to colorless was monitored by recording the UV-visible spectra for upto 1 h. In all the uncatalyzed reductions, equal volume of water was used in place of aqueous AgNPs. All the reactions were carried out in triplicate.

Result and Discussion

Characterization of f-AgNPs

The peaks at 4.95 and between 4.35-3.14 ppm in ^{1}H NMR of NG (Figure S7) correspond to methylene, hydroxyl, and α, β-methine protons of polysaccharide, amino sugars, proteinaceous amino acid and d-glucopyranosylfuranic acid contents of NG, respectively. The 5.6 and 1.91 ppm peaks infer anomeric proton of sugar and methyl protons, respectively, while peaks ≈5 ppm correspond to the amine protons from amino sugars and proteinaceous NG content. The ^{1}H NMR of AgNP (Figure S8) is similar to that of NG, depicting the presence of polysaccharide, amino sugars, and proteinaceous amino acid from NG at AgNP surface. For Ala-AgNP, a more intense peak at 1.33 ppm (Figure S9) assigned to methyl protons of Ala when compared with the ^{1}H NMR of NG, elucidate functionalization by Ala. The multiple peaks between 7-8 ppm in the ^{1}H NMR of Trp due to the indole group are absent in Trp-AgNP (Figure S10). The disappearance of these peaks infers that the protons responsible for coupling with adjacent protons are now engaged. Possibly, the electron cloud of these protons is hybridized strongly with the functional groups in NG constituents, wherein during Ag^+ ion reduction, the indole group undergoes modification (Figure S10, 7–8 ppm region), and Trp molecules may have polymerized to poly(2,6-indole).[1,2]

In the ^{1}H NMR of Met-AgNP (Figure S11), peaks at 2.19 and 2.67 ppm corresponding to methyl and methylene protons (-S-C) of Met, respectively, have shifted upfield when compared to Met (Figure S11, 1.98 and 2.49 ppm). For Met-AgNP, the methine proton (-S-C) peak at 3.72 ppm is more intense than for NG and AgNP, illustrating functionalization by Met. The peaks at 7.07 and 7.89 ppm in the ^{1}H NMR of His-AgNP (Figure S12) infers aromatic protons of imidazole group, which have shifted downfield when compared to His (Figure S12, 6.88 and 7.58 ppm), elucidating functionalization by His. In the ^{1}H NMR of Glu-AgNP (Figure S13), peaks at 1.98 and 2.26 ppm are assigned to methylene protons, whereas peak at 3.61 is assigned to methine

proton of Glu. For Glu-AgNP, peak at 2.40 ppm (protons coordinated to the α-carbon of the Glu) shifted upfield to 2.26 ppm, while the intensity of the peak at 3.61 ppm became more intense than in NG (Figure S13), illustrating functionalization by Glu. The peaks between 2.67 and 2.82 ppm in the ^{1}H NMR of Asp-AgNP (Figure S14) correspond to methylene protons of Asp. No peak shifting observed for Asp-AgNP when compared to Asp suggests similar functional activities by Asp. The peaks at 4.95 and between 4.35-3.14 ppm in the ^{1}H NMR of AgNP and f-AgNPs further confirmed their capping with polysaccharides and proteins of NG.

Table S1. The d-Spacing Values and Crystallite Size of Ag_2O and Ag Crystallites Present in AgNPs: AgNP, Ala-AgNP, Trp-AgNP, Met-AgNP, His-AgNP, Glu-AgNP, and Asp-AgNP; calculated using Debye–Scherrer equation

2θ	Plane	d-spacing (Standard)[3,4]	d-spacing (observed)	Size (nm)
		AgNP		
		Ag_2O		
28.1	110	0.33658	0.33726	123
32.5	111	0.27482	0.27562	45
46.4	211	0.19433	0.19588	129
54.9	220	0.16829	0.16721	30
57.5	309	N/A	0.16023	39
67.5	222	0.13741	0.13885	36
		Ag		
38.4	111	0.23480	0.23422	18
		Ala-AgNP		
		Ag_2O		
28.0	110	0.33658	0.33651	54
32.4	111	0.27482	0.27644	62
46.3	211	0.19433	0.19591	74
54.9	220	0.16829	0.16735	54
57.5	309	N/A	0.16027	45
67.4	222	0.13741	0.13894	57
		Ag		
38.5	111	0.23480	0.23398	18
44.6	200	0.20300	0.20309	11
64.8	220	0.14370	0.14394	14
		Trp-AgNP		
		Ag_2O		
27.9	110	0.33658	0.33644	54
32.3	111	0.27482	0.27691	41
46.1	211	0.19433	0.19697	26
54.7	220	0.16829	0.16790	33
57.3	309	N/A	0.16073	23
		Ag		
38.5	111	0.23480	0.23382	13
44.3	200	0.20300	0.20450	11
64.8	220	0.14370	0.14392	12
77.7	311	0.12290	0.12291	17
		Met-AgNP		
		Ag_2O		
28.1	110	0.33658	0.33776	35
32.6	111	0.27482	0.27509	35
46.6	211	0.19433	0.19505	74
55.1	220	0.16829	0.16681	54
57.7	309	N/A	0.15986	30
67.7	222	0.13741	0.13849	24

		Ag		
38.6	111	0.23480	0.23335	10
65.0	220	0.14370	0.14349	18
		His-AgNP		
		Ag_2O		
28.2	110	0.33658	0.33684	61
32.5	111	0.27482	0.27541	28
46.5	211	0.19433	0.19546	32
55.1	220	0.16829	0.16674	11
57.7	309	N/A	0.15987	23
		Ag		
38.5	111	0.23480	0.23399	14
44.5	200	0.20300	0.20358	8
64.8	220	0.14370	0.14379	14
78.0	311	0.12290	0.12255	15
81.9	222	0.11750	0.11752	6
		Glu-AgNP		
		Ag_2O		
28.0	110	0.33658	0.33691	61
32.3	111	0.27482	0.27683	49
46.3	211	0.19433	0.19623	129
54.8	220	0.16829	0.16751	45
57.4	309	N/A	0.16049	30
67.4	222	0.13741	0.13898	36
		Ag		
38.4	111	0.23480	0.23433	11
64.8	220	0.14370	0.14393	12
77.6	311	0.12290	0.12300	19
		Asp-AgNP		
		Ag_2O		
28.1	110	0.33658	0.33717	61
32.5	111	0.27482	0.27529	62
46.5	211	0.19433	0.19545	65
55.0	220	0.16829	0.16700	54
57.6	309	N/A	0.15991	77
67.6	222	0.13741	0.13867	71
		Ag		
38.5	111	0.23480	0.23399	18
64.9	220	0.14370	0.14370	23

Table S2. Measured XPS Data from Ag 3d, C 1s, O 1s, and N 1s Spectra

	AgNP	Asp-AgNP	Met-AgNP	His-AgNP	Trp-AgNP	Glu-AgNP	Ala-AgNP
	Binding Energy (eV)						
	366.9	367.5	364	364.4	366.4	367.2	367.3
	368.1	368.9	368.4	368.9	368.2	368.4	368.8
	372.7	373.5	372.6	372.3	372.5	373.1	373.2
Ag 3d	374.1	374.9	374.5	374.9	374.1	374.3	374.7
	281.6	283.3	284.4	285.1	284.9	283.3	284.4
	284.8	285.5		290.5	287.8	286.1	
C 1s		289.1				289.2	
	529.6	531.2	528.1	530.5	530.3	529.8	530.3
	531.5	532.8	529.3	532.4	532	531.5	531.5
			531.4	534.4		532.8	532.7
O 1s			532.3				
	398.8	399.2	399	396.6	397.1	399.6	398.6
			400.1	399.1	399.5	401	
N 1s					402.4		

Table S3. Percentage of Ag^0 and Ag_2O Content in AgNPs Calculated from XPS Analysis and UV-visible Absorbance Spectra

AgNPs	(%) Ag^0 from XPS	(%) Ag_2O from XPS	(%) Ag^0 from Absorbance spectra	(%) Ag_2O from Absorbance spectra
AgNP	33.53	66.47	36.33	63.67
Ala-AgNP	37.52	62.48	41.03	58.97
Trp-AgNP	76.84	23.16	85.68	14.32
Met-AgNP	71.36	28.64	79.08	20.92
His-AgNP	73.89	26.11	84.58	15.42
Glu-AgNP	59.09	40.91	65.97	34.03
Asp-AgNP	38.87	61.13	45.74	54.26

Table S4. Summary of the Amount of MB, Amount of Reducing Agent and Amount of Catalyst Used in MB Reduction from Literature

Catalyst	Amount of MB (mg)	Amount of reducing agent (μmol)	Amount of catalyst used	MB removal (%)	Time	Refs
Au–CNx composite	0.030	visible light	1 mg	96%	120 min	5
TiO_2 (P25)-graphene	0.345	UV	30 mg	70-85%	55 min	6
AuNP	0.500	400 μmol $NaBH_4$	1 mg	100%	8 min	7
AgNP	0.300	158.6 μmol $NaBH_4$	-	100%	8-20 min	8
AuNP	0.330	211.5 μmol $NaBH_4$	-	100%	4-12 min	8
AgNP	0.320	100 μmol $NaBH_4$	≈ 0.07 mg	100%	8-19 min	9
AgNP	0.320	845.5 μmol $NaBH_4$	≈ 0.07 mg	100%	8-12 min	10
Ag–In–Ni–S	3.199	sunlight	20 mg	100%	2 min	11
AgNP	0.480	10 μmol $NaBH_4$	11 mg	100%	15 min	12
AuNP	0.008	10 μmol $SnCl_2$	0.065 mg	100%	10-35 min	13
p(TA)–Cu ILs composite	10.235	1982.6 μmol $NaBH_4$	0.0039 mmol	100%	3 min	14
GT-Fe NPs	2.303	5.0 mL 10.0% H_2O_2	50.0 mg	≈50%	5 min	15
Ni NS	0.026	0.04 μmol $NaBH_4$	0.2 mg	100%	40 sec	16
Cu_2O@Ag	0.058	6 μmol $NaBH_4$	0.1 mg	80%	5-9 min	17
AgNPs-Fe_3O_4@PDA	0.150	50 μmol $NaBH_4$	5 mg	100%	30 min	18
AgNPs/P(NIPAM-co-DMA) microgels	0.015	105.7 μmol $NaBH_4$	0.056 mg	100%	28 min	19
Sacha inchi (SI) oil templated AgNPs	0.050	Sunlight	≈0.022 mg	95%	480 min	20
Graphene oxide (GO)/AgNPs	0.480	10 μmol $NaBH_4$	≈0.054 mg	100%	15 min	21
Ag colloid	0.032	0.75 μmol $NaBH_4$	0.1 mg	65%	10 min	22
Au-PBCGO55	0.010	100 μmol $NaBH_4$	0.003	83%	33 min	23
Ag-PBCGO55	0.010	100 μmol $NaBH_4$	0.003	≈69%	18 min	23
AgDENs	0.001	0.3264 mg H_2O_2	0.15 mL 0.25 μ M	≈70%	150 min	24
AuDENs	0.001	0.3264 mg H_2O_2	0.15 mL 0.25 μ M	≈83%	150 min	24
Fe_3O_4@Tween20@Ag	0.320	10 μmol $NaBH_4$	5 mg	≈93%	17 min	25
AgNPs (in 0.01 M aq. AOT)	0.011	10 μmol $SnCl_2$	0.01 mg	100%	4 min	This work
AgNPs (in 0.01 M aq. SDS)	0.011	10 μmol $SnCl_2$	0.01 mg	100%	4 min	This work
AgNPs (in 0.01 M aq. DTAB)	0.011	10 μmol $SnCl_2$	0.01 mg	100%	5 min	This work
AgNPs (in aq.)	0.011	10 μmol $SnCl_2$	0.01 mg	100%	7 min	This work
Trp-AgNPs (in aq and 0.01 M aq. AOT/SDS/DTAB/T-20))	0.011	10 μmol $SnCl_2$	0.01 mg	100%	40 sec	This work

Table S5. Summary of the Activity Parameter (κ), Dependent on the Rate Constants of the Reaction (k_1) and the Amounts of Catalyst Used for CR Reduction

Catalyst	Amount of catalyst (mg)	k_1 (sec^{-1})	κ ($s^{-1}\cdot g^{-1}$)	Refs
AuNP	1	0.0041	4.1	26
Ag/GO–Chitosan	5	0.0034	0.68	27
Au/GO–Chitosan	5	0.0021	0.428	27
NiS	100	0.0003	0.0029	28
Titanium oxide nanotube arrays	-	0.0002	-	29
CuO nanowires	-	0.0001	-	30
ZnO@CuO nanostructures	-	0.0001	-	30
Fe3O4@CuO nanostructures	-	0.0001	-	30
Ag/GO-G3PAMAM	5	0.0168	3.36	31
Ag/GO-G2PAMAM	5	0.0109	2.18	31
Ag/GO-G1PAMAM	5	0.0048	0.96	31
Au/GO-G3PAMAM	5	0.0121	2.42	31
AgNP	0.011	0.0041	376.67	This work
Ala-AgNP	0.011	0.0025	225.15	This work
Trp-AgNP	0.011	0.0003	23.03	This work
Met-AgNP	0.011	0.0002	22.12	This work
His-AgNP	0.011	0.0020	185.15	This work
Glu-AgNP	0.011	0.0019	176.06	This work
Asp-AgNP	0.011	0.0037	334.85	This work

Table S6. Summary of the Activity Parameter (κ), Dependent on the Rate Constants of the Reaction (k_1) and the Amounts of Catalyst Used for 4-NP Reduction

Catalyst	Amount of catalyst	k_1 (sec^{-1})	κ ($s^{-1}\cdot g^{-1}$)	Refs
AuNPs	3.29	0.0120	3.65	32
Spongy AuNPs	6	0.0021	0.35	33
AuNPs	1.99	0.1699	85.44	34
Au/graphene	0.1	0.0032	31.70	35
Carbon@AuNPs	0.1	0.0054	54.20	36
TAC-Ag-1.0	4	0.0052	1.30	37
TAC-Ag-1.4	5	0.0017	0.41	37
TSC-Ag-1.4	6	0.0004	0.09	37
Ag-NP/C composite	1	0.0017	1.69	38
Fe3O4-@SiO2-Ag	1	0.0077	7.67	39
CNFs@Au	0.1	0.0054	54.20	40
Pd-Au@MWCNT	0.02	0.0018	90.50	41
GO–Chit-AgNPs	5	0.0055	1.10	42
GO–Chit-AuNPs	5	0.0038	0.76	42
SMG-capped AgNPs	0.32	0.0009	2.83	43
glucan-AuNPs	3.5	0.0019	0.54	44
Ala-AgNP	0.011	0.0012	110.45	This work
Met-AgNP	0.011	0.0012	112.27	This work
His-AgNP	0.011	0.0003	25.61	This work
Glu-AgNP	0.011	0.0007	60.15	This work
Asp-AgNP	0.011	0.0009	81.97	This work

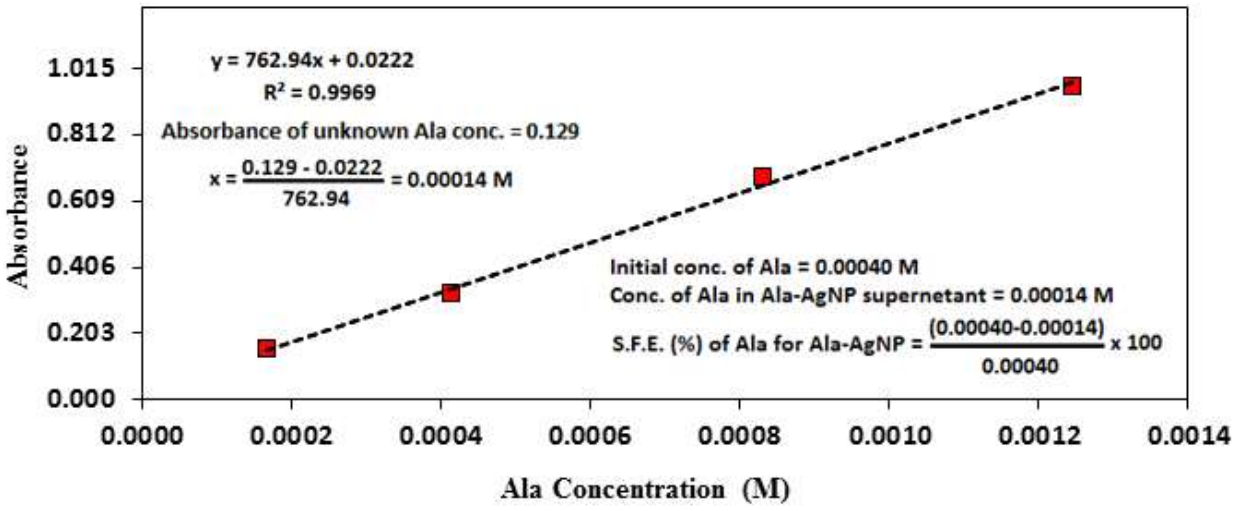

Figure S1. Standard curve of alanine-ninhydrin complex

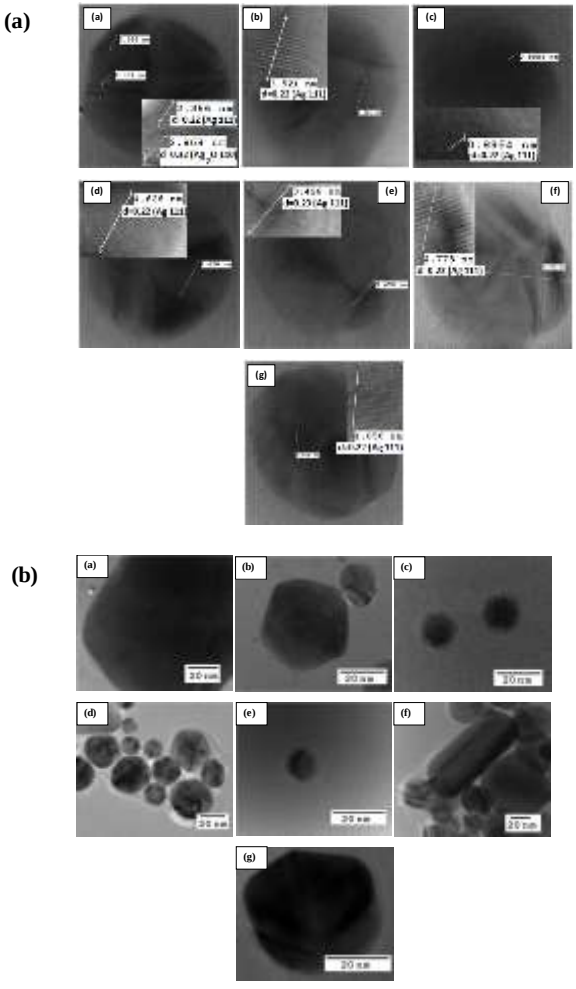

Figure S2. HR-TEM micrograph of (a) AgNP (b) Ala-AgNP (c) Trp-AgNP (d) Met-AgNP (e) His-AgNP (f) Glu-AgNP (g) Asp-AgNP, illustrating capping and lattice spacing of Ag (111)/Ag2O (110) plane

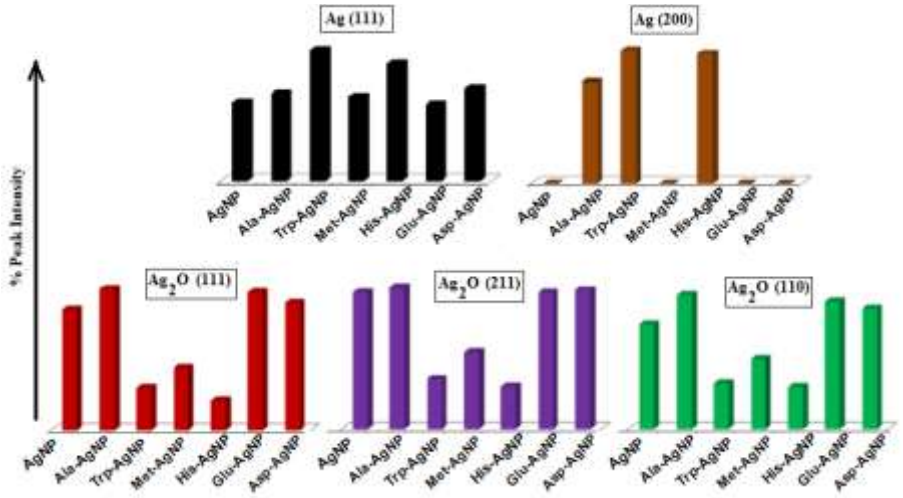

Figure S3. Percentage of XRD peak intensities of various Ag and Ag_2O crystallite lattice planes present in the AgNPs: AgNP, Ala-AgNP, Trp-AgNP, Met-AgNP, His-AgNP, Glu-AgNP, and Asp-AgNP

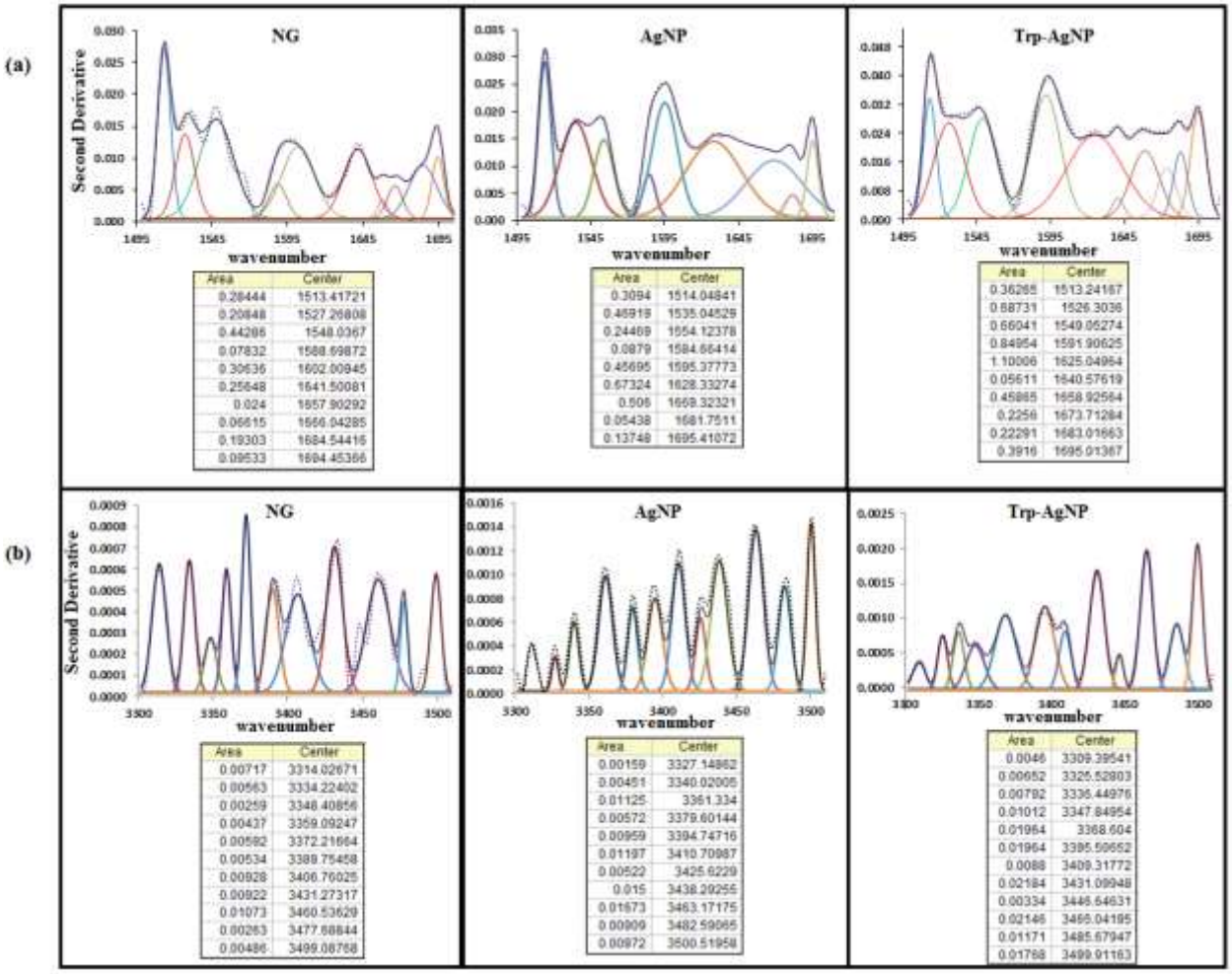

Figure S4. Comparative deconvoluted FTIR spectrums of NG, AgNP and Trp-AgNP at specific wavenumber range (a) 1500-1700 cm^{-1} and (b) 3300-3500 cm^{-1}

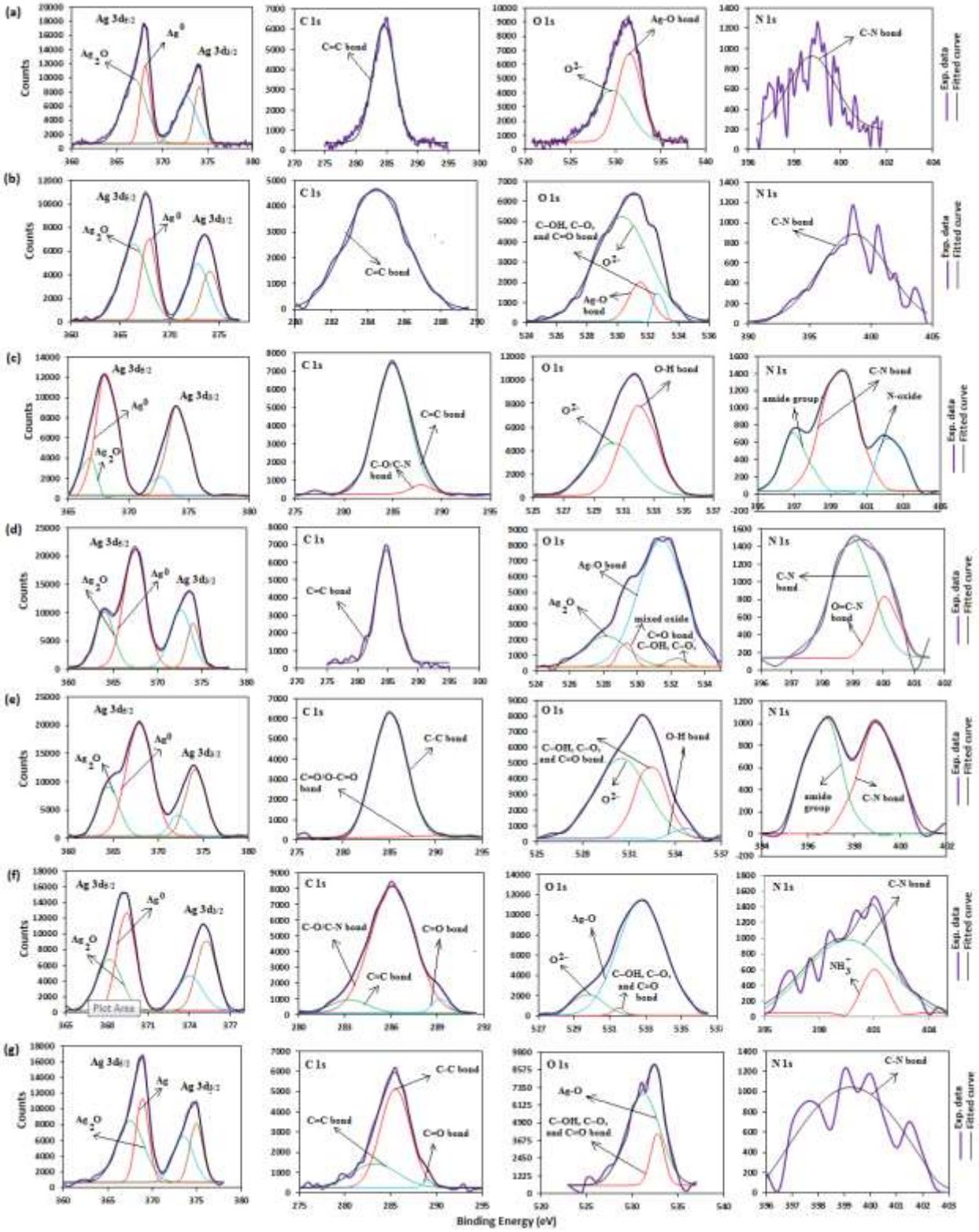

Figure S5. XPS spectral analysis of (a) AgNP (b) Ala-AgNP (c) Trp-AgNP (d) Met-AgNP (e) His-AgNP (f) Glu-AgNP and (g) Asp-AgNP showing corresponding deconvoluted peaks in the high resolution spectra of various elements present, i.e., Ag (3d), O (1s), C (1s), and N (1s)

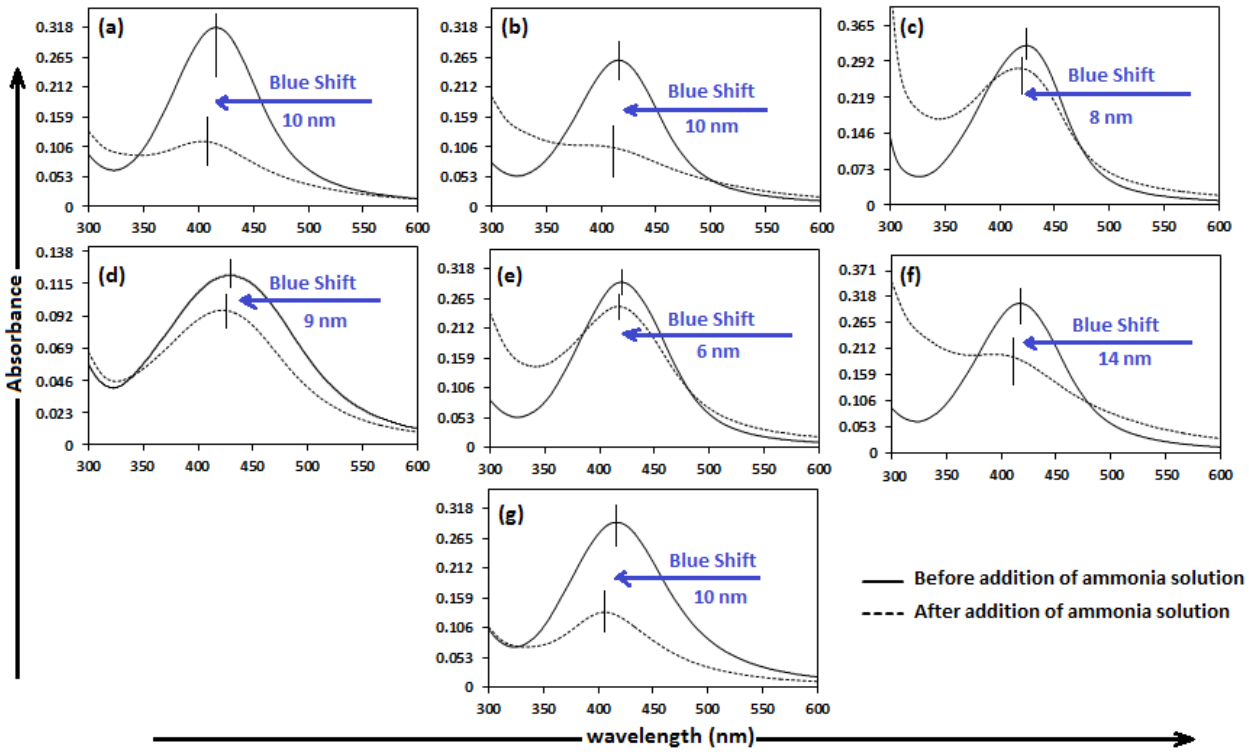

Figure S6. UV-visible absorbance spectra of (a) AgNP (b) Ala-AgNP (c) Trp-AgNP (d) Met-AgNP (e) His-AgNP (f) Glu-AgNP and (g) Asp-AgNP dispersion in absence and presence of aqueous ammonia

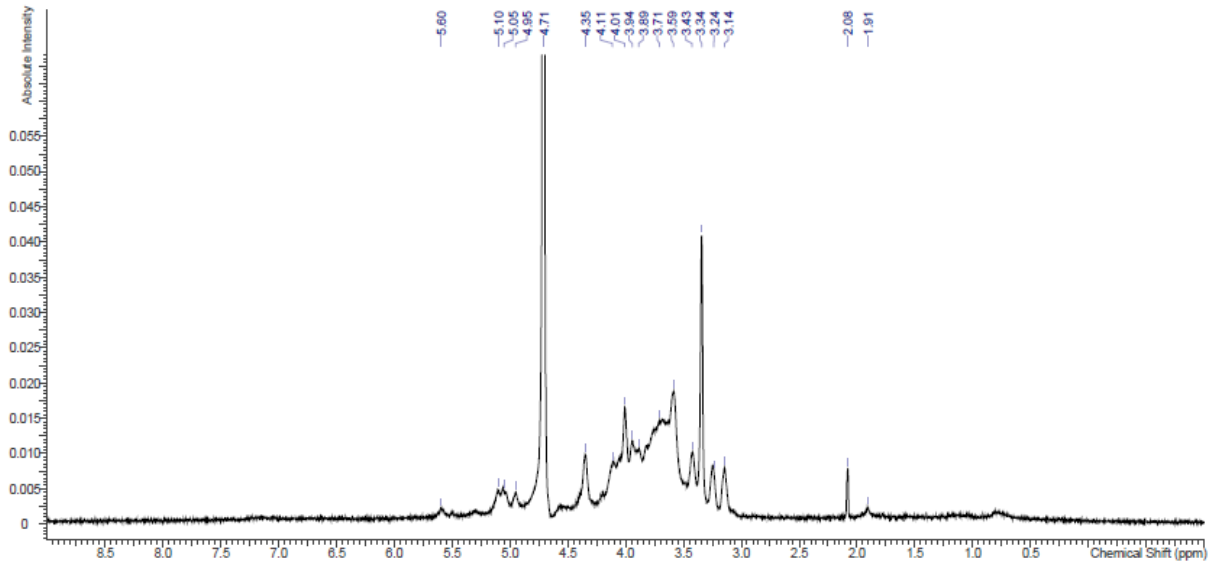

Figure S7. ^{1}H NMR spectrum of NG in D_2O at 500 MHz

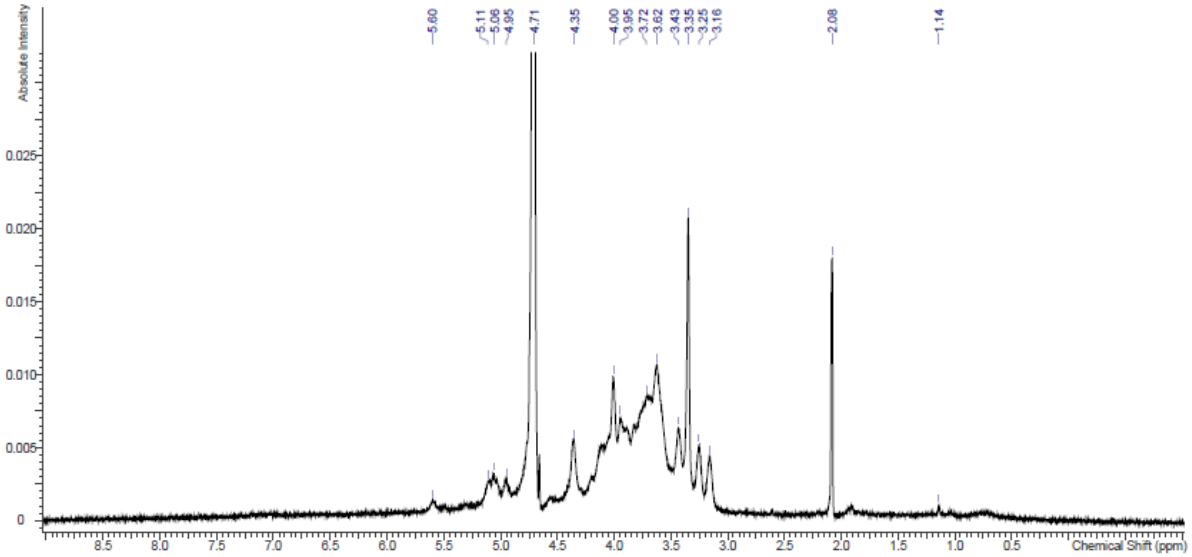

Figure S8. ^{1}H NMR spectrum of AgNP in D_2O at 500 MHz

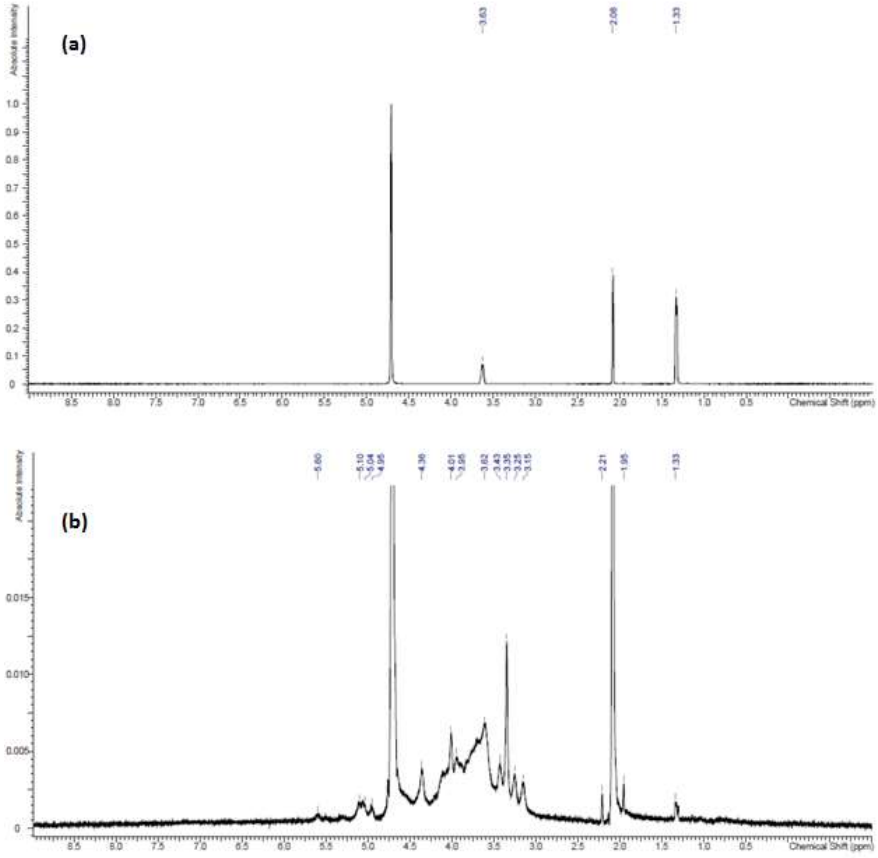

Figure S9. ^{1}H NMR spectrum of (a) Ala and (b) Ala-AgNP in D_2O at 500 MHz

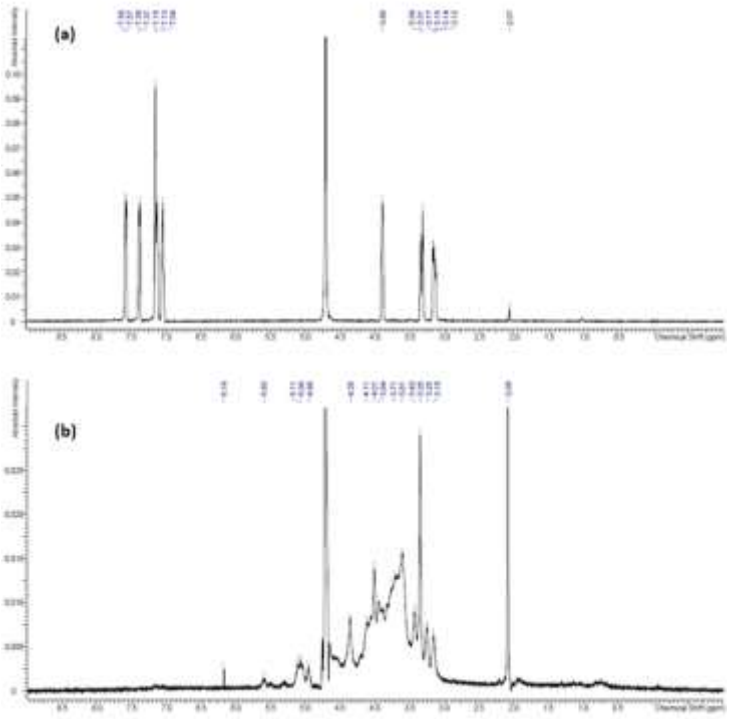

Figure S10. ^{1}H NMR spectrum of (a) Trp and (b) Trp-AgNP in D_2O at 500 MHz

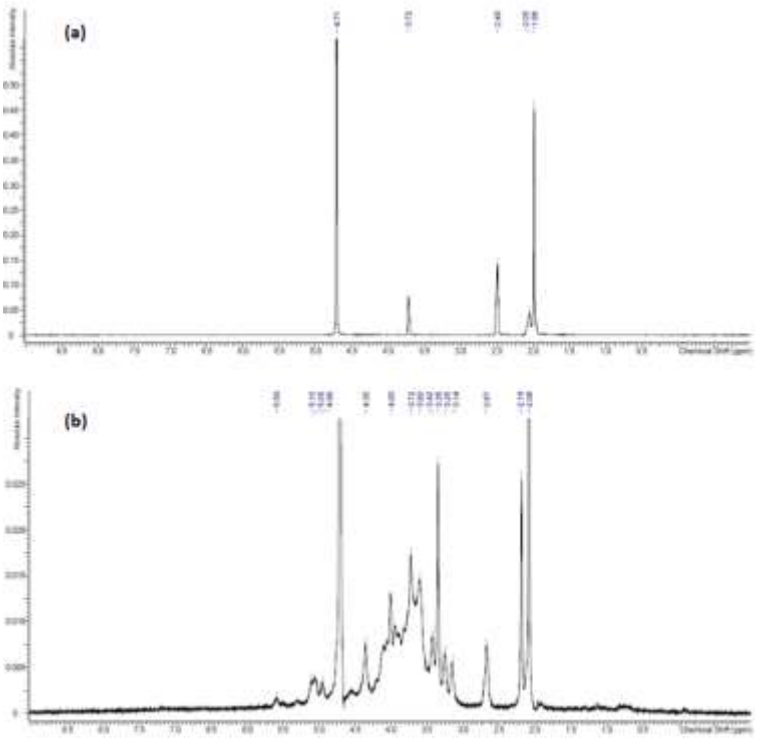

Figure S11. ^{1}H NMR spectrum of (a) Met and (b) Met-AgNP in D_2O at 500 MHz

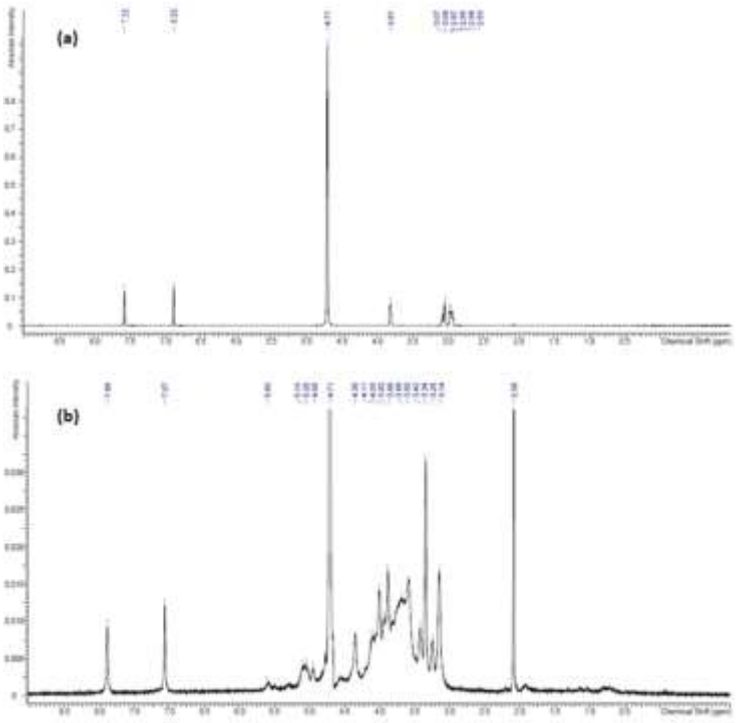

Figure S12. ^{1}H NMR spectrum of (a) His and (b) His-AgNP in D_2O at 500 MHz

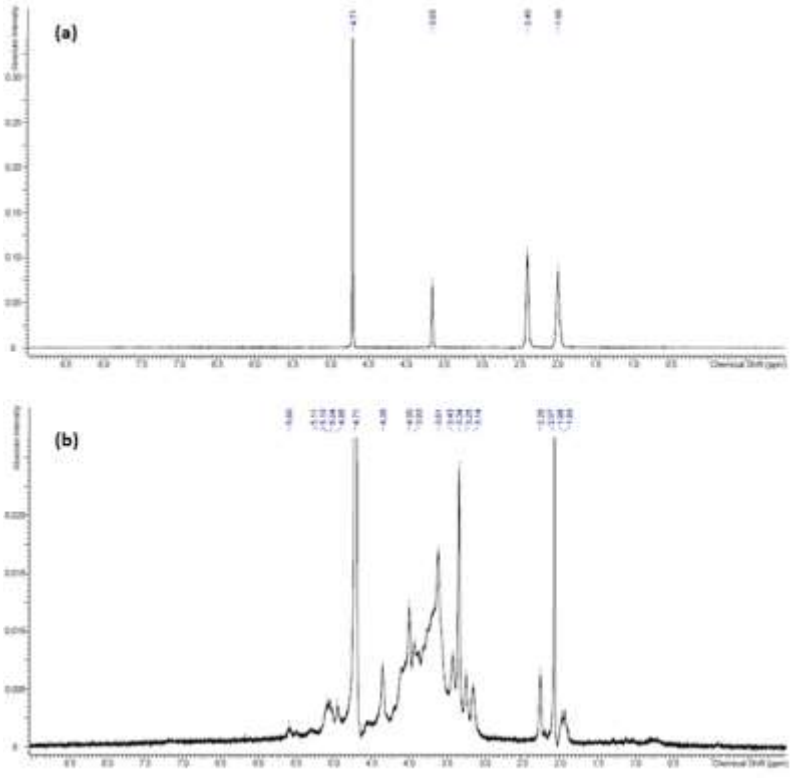

Figure S13. ^{1}H NMR spectrum of (a) Glu and (b) Glu-AgNP in D_2O at 500 MHz

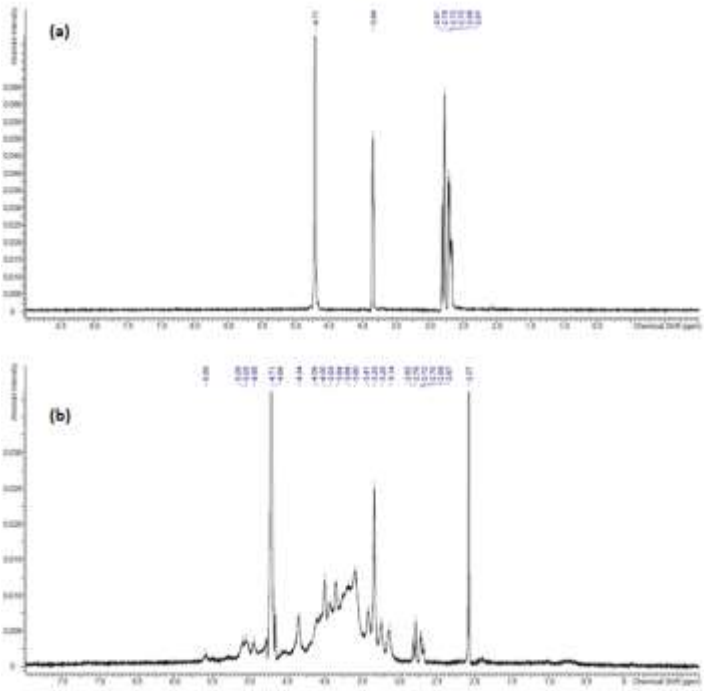

Figure S14. ^{1}H NMR spectrum of (a) Asp and (b) Asp-AgNP in D_2O at 500 MHz

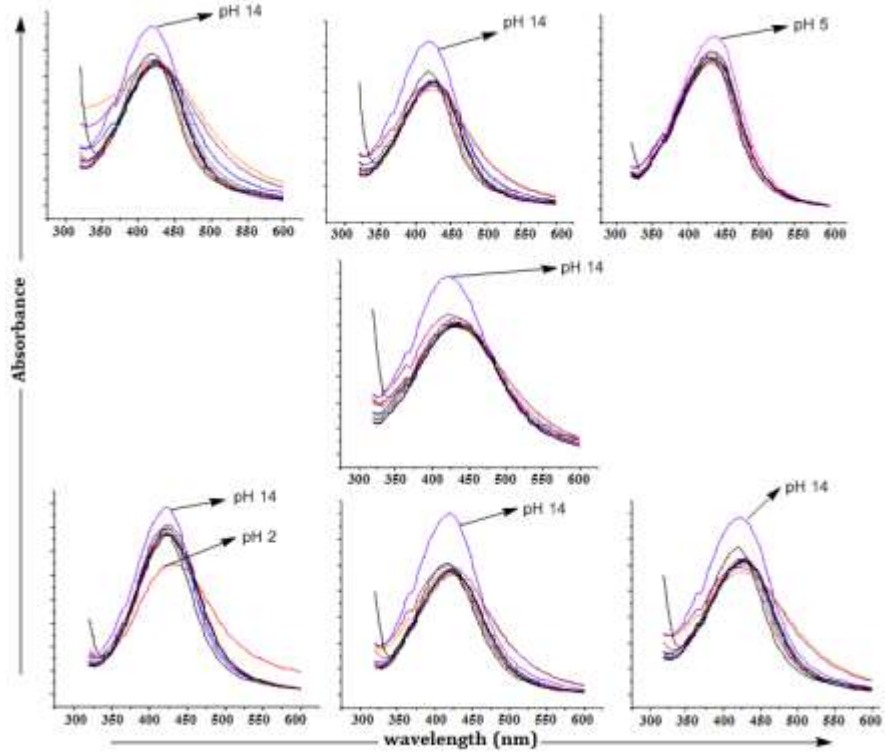

Figure S15. UV-visible absorption spectra of AgNPs: (a) AgNP (b) Ala-AgNP (c) Trp-AgNP (d) Met-AgNP (e) His-AgNP (f) Glu-AgNP (g) Asp-AgNP; in aqueous solutions of pH ranging from 2-14

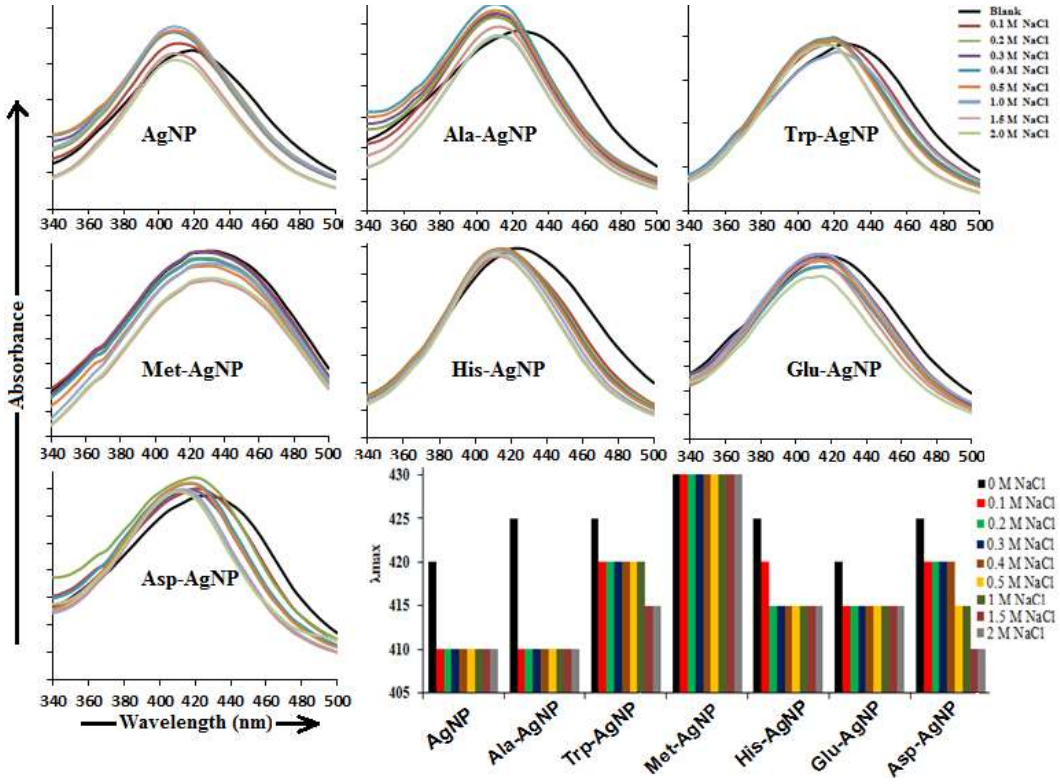

Figure S16. UV-visible absorption spectra of AgNPs in 0–2 M aqueous NaCl

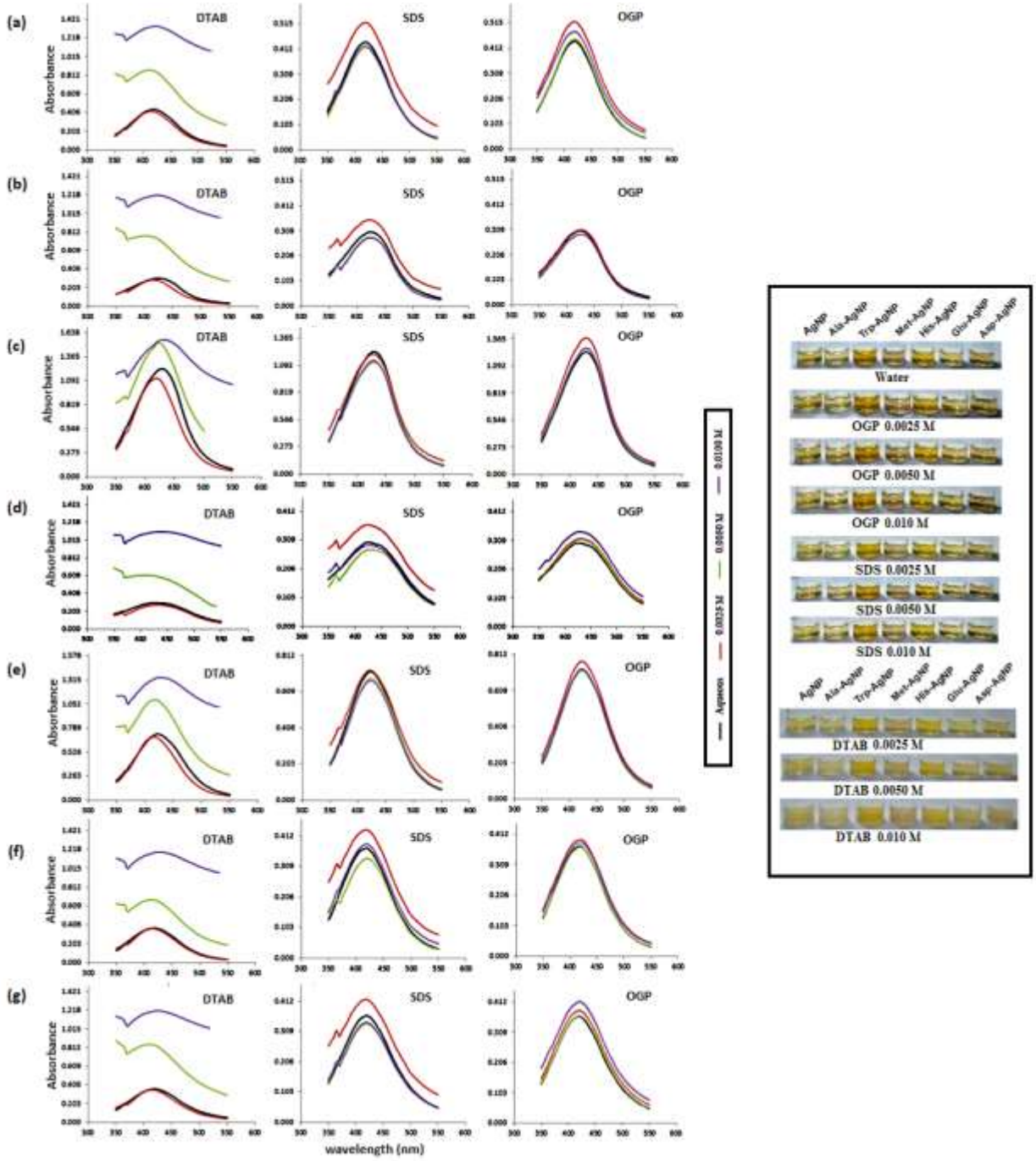

Figure S17. UV-visible spectra of (a) AgNP (b) Ala-AgNP (c) Trp-AgNP (d) Met-AgNP (e) His-AgNP (f) Glu-AgNP (g) Asp-AgNP; in 0.0025–0.010 mol·L^{-1} aqueous surfactants

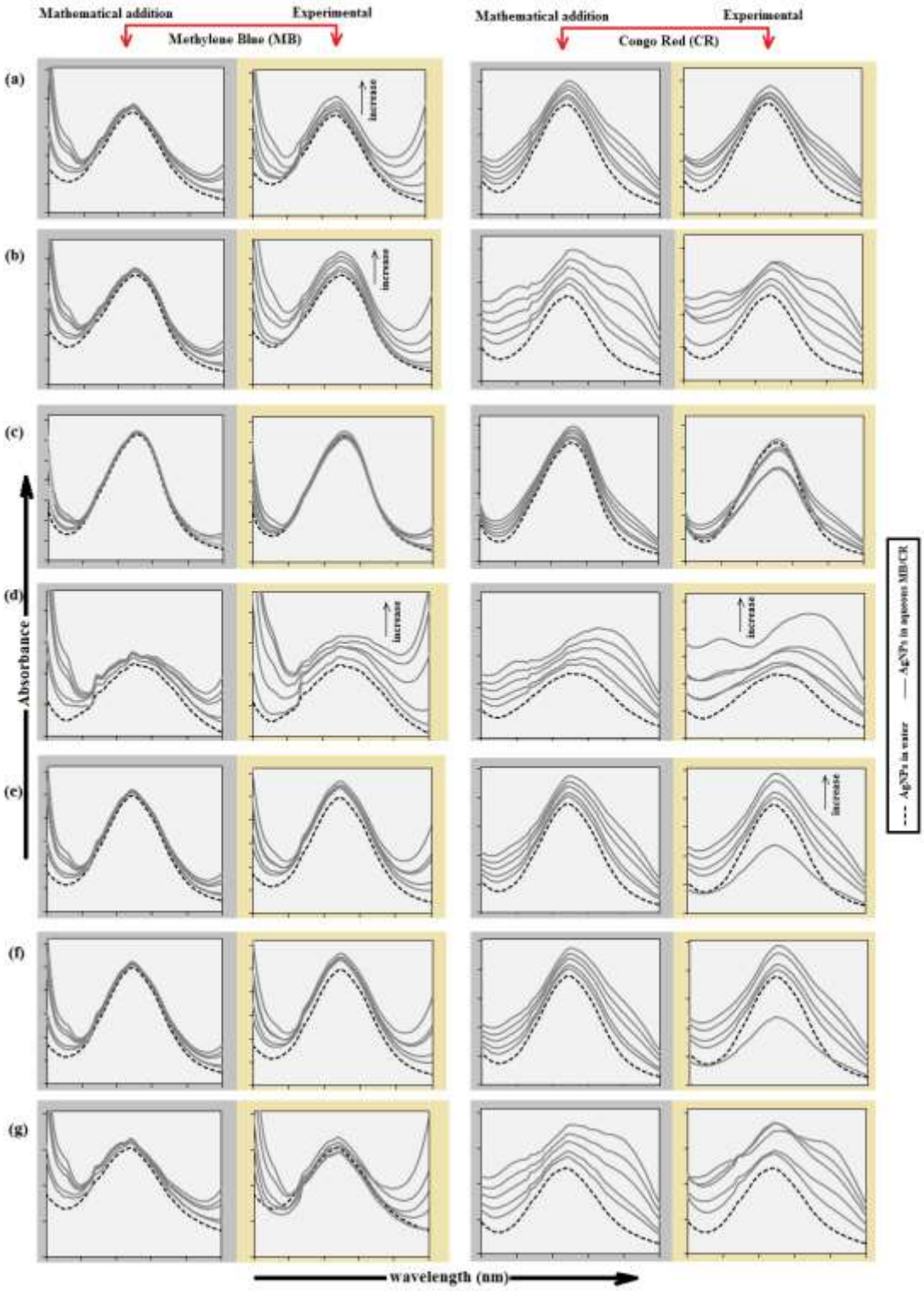

Figure S18. UV-visible spectra of (a) AgNP (b) Ala-AgNP (c) Trp-AgNP (d) Met-AgNP (e) His-AgNP (f) Glu-AgNP (g) Asp-AgNP; in presence of 0-50 μM aqueous MB/CR

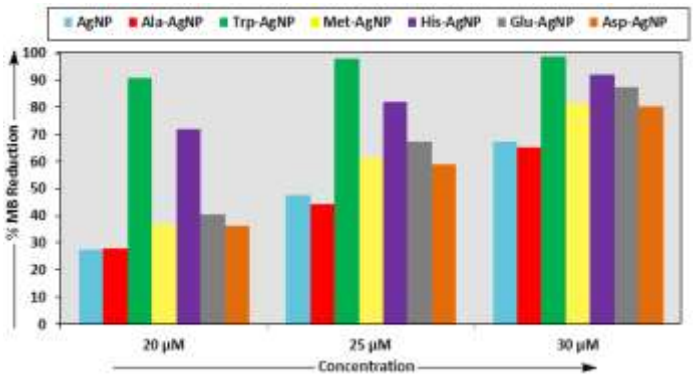

Figure S19. Percentage of MB reduced by acidic $SnCl_2$ after 3 min of catalysis in presence of (20-30 µM) AgNPs: AgNP, Ala-AgNP, Trp-AgNP, Met-AgNP, His-AgNP, Glu-AgNP, and Asp-AgNP; in T-20 micellar medium

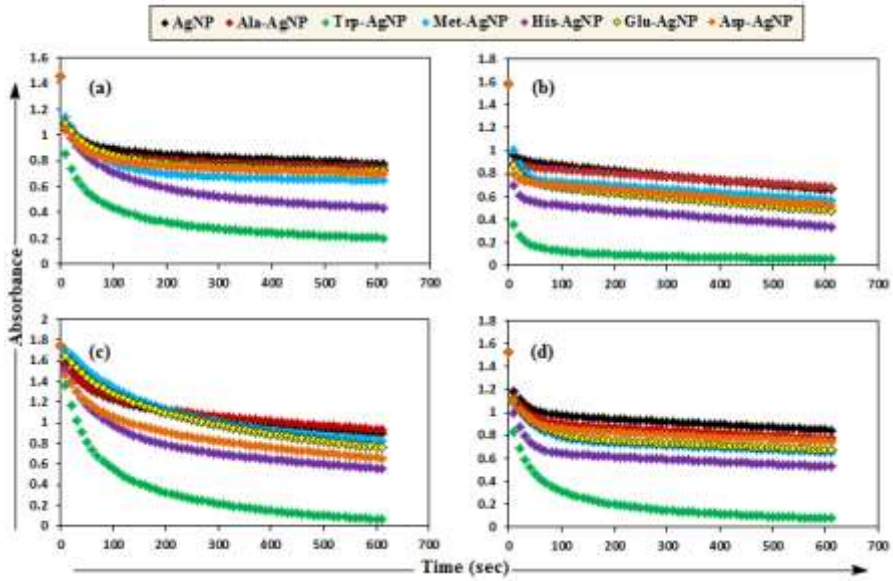

Figure S20. Plot of the absorbance at λ_{max} of MB versus time with 20 µM AgNPs in (a) in 0.01 M aqueous AOT (b) in 0.01 M aqueous SDS (c) in 0.01 M aqueous DTAB (d) in aqueous

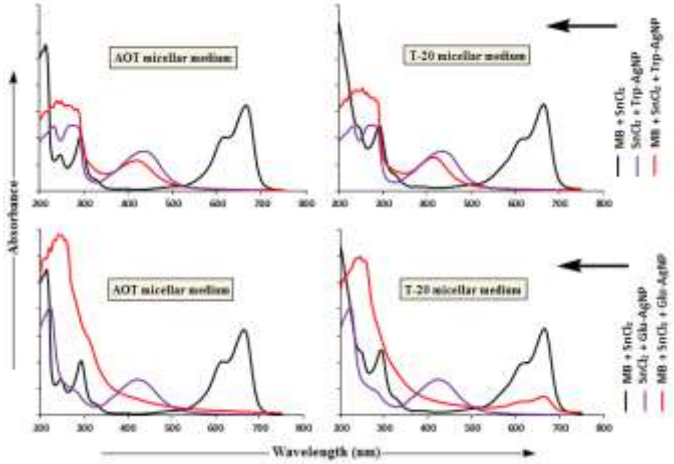

Figure S21. UV-visible absorbance spectra of reaction mixture containing MB and acidic $SnCl_2$ in AOT and T-20 micellar mediums, recorded 20 min after addition of Trp-AgNP and Glu-AgNP

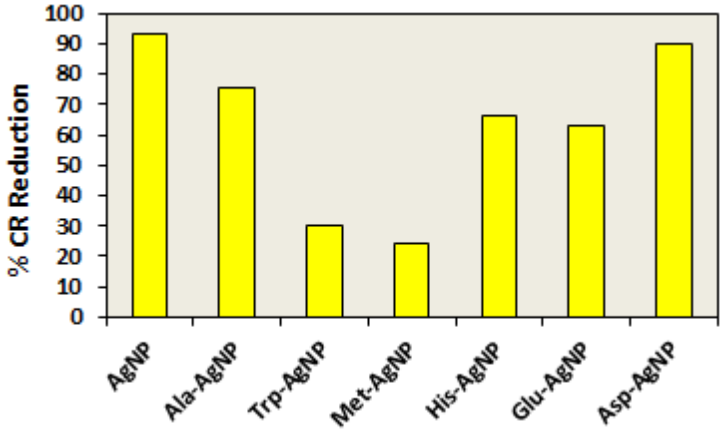

Figure S22. Percentage of CR reduced by $NaBH_4$ after 15 min of catalysis in presence of 30 μM AgNPs: AgNP, Ala-AgNP, Trp-AgNP, Met-AgNP, His-AgNP, Glu-AgNP, and Asp-AgNP

REFERENCES

[1] S. Selvan, *J. Chem. Soc. Chem. Commun.*, 1998, 0, 351-352.

[2] P. Selvakannan, S. Mandal, S. Phadtare, A. Gole, R. Pasricha, S. Adyanthaya and M. Sastry, *J. Colloid Interface Sci.*, 2004, 269, 97–102.

[3] L. Xu, B. Wei, W. Liu, H. Zhang, C. Su and J. Che, *Nanoscale Res. Lett.*, 2013, 8:536.

[4] W. Wei, X. Mao, L. Ortiz and D. Sadoway, *J. Mater. Chem.*, 2011, 21, 432–438.

[5] T. Bhowmik, M.K. Kundu and S. Barman, *RSC Adv*., 2015, 5, 38760–38773.

[6] H. Zhang, X. Lv, Y. Li, Y. Wang and J. Li, *ACS Nano*, 2010, 4(1), 380-386.

[7] B. Paul, B. Bhuyan, D.D. Purkayastha, S. Vadivel and S.S. Dhar, *Mater. Lett.*, 2016, 185, 143-147.

[8] V.S. Suvith and D. Philip, *Spectrochim. Acta Mol. Biomol. Spectrosc.*, 2014, 118, 526–532.

[9] V.K. Vidhu and D. Philip, *Micron*, 2014, 56, 54–62.

[10] V.K. Vidhu and D. Philip, *Micron*, 2014, 117, 102-108.

[11] A. Molla, M. Sahu and S. Hussain, *J. Mater. Chem. A*, 2015, 3, 15616–15625.

[12] M.K. Indana, B.R. Gangapuram, R. Dadigala, R. Bandi, and V. Guttena, *J. of Anal. Sci. Tech.*, 2016, 7:19.

[13] N. Gupta, H.P. Singh and R.K. Sharma, *Colloids Surf., A*, 2010, 367, 102–107.

[14] N. Sahiner, S. Sagbas and N. Aktas, *RSC Adv*., 2015, 5, 18183–18195.

[15] T. Shahwana, S.A. Sirriah, M. Nairat, E. Boyacı, A.E. Eroglu, T.B. Scott and K.R. Hallam, *Chem. Eng. J*., 2011, 172, 258– 266.

[16] N.H. Kalwar, Sirajuddin, R.A. Soomro, S.T.H. Sherazi, K.R. Hallam and A.R. Khaskheli, *International Journal of Metals* 2014, Article ID 126103, 10 pages.

[17] S. Kandula and P. Jeevanandam. *Eur. J. Inorg. Chem*., 2016, 10, 1548–1557.

[18] M. Wu, Y. Li, R. Yue, X. Zhang and Y. Huang, *Scientific Reports*, 2017, 7:42773.

[19] Y. Tang, T. Wu, B. Hu, Q. Yang, L. Liu, B. Yu, Y. Ding and S. Ye, *Mater. Chem. Phy*., 2015, 149–150, 460–466.

[20] B. Kumar, K. Smita, L. Cumbal and A. Debut, *Ind. Crop. Prod*., 2014, 58, 238–243.

[21] T.V.M. Sreekanth, M.J. Jung and I.Y. Eom, *Appl. Sur. Sci*., 2016, 61, 102–106.

[22] C. Wen, M. Shao, S. Zhuo, Z. Lin, and Z. Kang, *Mater. Chem. Phy*., 2012, 135, 780–785.

[23] K.Y. Cho, H.Y. Seo, Y.S. Yeom, P. Kumar, A.S. Lee, K.Y. Baek and H.G. Yoon, *Carbon*, 2016, 105, 340–352.

[24] A.K. Ilunga and R. Meijboom, *J. Mol. Catal. A*, 2016, 411, 48–60.

[25] U. Kurtan, A. Baykal and H. Sözeri, *J. Inorg. Organomet. Polym,*, 2015, 25, 921–929.

[26] B. Paul, B. Bhuyan, D.D. Purkayastha, S. Vadivel and S.S. Dhar, *Mater. Lett*., 2016, 185, 143–147.

[27] R. Rajesh, E. Sujanthi, S.S. Kumar and R. Venkatesan, *Phys. Chem. Chem. Phys*., 2015, 17, 11329-11340.

[28] H. Guo, Y. Ke, D. Wang, K. Lin, R. Shen, J. Chen and W. Weng, *J. Nanopart. Res.*, 2013, 15(3):1475.

[29] T.S. Natarajan, K. Natarajan, H.C. Bajaj and R.J. Tayade, *Ind. Eng. Chem. Res.* **2011**, *50*, 7753–7762.

[30] D. Malwal and P. Gopinath, *Catal. Sci. Technol*., 2016, 6, 4458-4472.

[31] R. Rajesh, S.S. Kumar and R. Venkatesan, *New J. Chem*., 2014, 38, 1551-1558.

[32] M. Rashid and T.K. Mandal, *Adv. Funct. Mater*., 2008, 18, 2261–2271.

[33] M.H. Rashid, R.R. Bhattacharjee, A. Kotal and T.K. Mandal, *Langmuir*, 2006, 22, 7141–7143.

[34] S.K. Das, C. Dickinson, F. Lafir, D.F. Brougham and E. Marsili, *Green Chem*., 2012, 14, 1322–1334.

[35] J. Li, C.Y. Liu and Y Liu, *J. Mater. Chem*., 2012, 22, 8426–8430.

[36] P. Zhang, C.L. Shao, X.H. Li, M.Y. Zhang, X. Zhang, C.Y. Su, N. Lu, K.X. Wang and Y.C. Liu, *Phys. Chem. Chem. Phys*., 2013, 15, 10453–10458.

[37] M.H. Rashid and T.K. Mandal, *J. Phys. Chem. C*, 2007, 111, 16750−16760.

[38] S. Tang, S. Vongehr and X. Meng, *J. Phys. Chem. C*, 2010, 114, 977−982.

[39] Y. Chi, Q. Yuan, Y. Li, J. Tu, L. Zhao, N. Li and X. Li, *J. Colloid Interface Sci*., 2012, 383, 96−102.

[40] P. Zhang, C. Shao, X. Li, M. Zhang, X. Zhang, C. Su, N. Lu, K. Wang and Y. Liu, *Phys. Chem. Chem. Phys*., 2013, 15, 10453–10458.

[41] C.H. Liu, J. Liu, Y.Y. Zhou, X.L. Cai, Y. Lu, X. Gao and S.D. Wang, *Carbon*, 2015, 94, 295–300.

[42] R. Rajesh, E. Sujanthi, S.S. Kumar and R. Venkatesan, *Phys. Chem. Chem. Phys*., 2015, 17, 11329-11340.

[43] M. Krishna, G.B. Reddy, G. Veerabhadram and A. Madhusudhan, *Appl Nanosci*, 2016, 6, 681–689.

[44] I.K. Sen, K. Maity and S.S. Islam, *Carbohydr. Polym*., 2013, 91, 518– 528.

ELECTRONIC SUPPLEMENTARY INFORMATION

Biosynthesis of Amino Acid Functionalized Silver Nanoparticles for Potential Catalytic and Oxygen Sensing Applications

Abhishek Chandra[†] and Man Singh[†*]

[†]School of Chemical Sciences, Central University of Gujarat, Gandhinagar-382030, India

Email: mansingh50@hotmail.com, abhishekchandra.15@gmail.com

EXPERIMENTAL SECTION

Estimation of Total Silver Concentration in AgNPs

On completion of the reaction, AgNPs were separated by centrifugation at 17500×g for 20 min. The precipitated AgNPs were collected and digested in aqua regia. The concentration of the Ag^+ ions was measured in triplicate by induced couple plasma-optical emission spectrometer (ICP-OES) (Varian Spectra AA 55, USA) against a standard $AgNO_3$ solution. The concentration of Ag was 1.68 mM in 100 ml aqueous AgNPs dispersion.

Influence of pH, Ionic Strength, Surfactants and Dyes on AgNPs Stability

The colloidal stability of AgNPs at variable pH was studied by recording the UV-visible spectra of 100 μM AgNPs dispersion in the pH range 2–10. The pH of AgNPs dispersion was varied by adding different volumes of 0.1 M aqueous HCl/NaOH. The colloidal stability of AgNPs with increasing ionic strength of the dispersion was studied by recording the UV-visible spectra of 100 μM AgNPs in 0.1 to 2 M aqueous NaCl. The colloidal stability of AgNPs in aqueous surfactants was studied by recording the UV-visible spectra of 30 μM AgNPs in 0.0025 to 0.010 M aqueous cationic surfactant (DTAB), anionic surfactant (SDS), and non-ionic surfactant (OGP). The colloidal stability of AgNPs in aqueous dyes was studied by recording the UV-visible spectra of 30 μM AgNPs dispersion in 10 to 50 μM aqueous cationic dyes (MB) and anionic dye (CR).

For all the colloidal stability experiments, the UV-visible spectra were recorded after 30 min of AgNPs addition to the various aqueous medium. All the experiments were carried out in triplicate.

Catalytic Activity of AgNPs

The AgNPs catalytic activity on MB reduction by acidic $SnCl_2$, while CR and 4-NP reduction by $NaBH_4$ was monitored by UV-visible spectroscopy. For MB reduction, the reactions were carried out in water and in 0.01 M aqueous DTAB/SDS/AOT/T-20. Briefly, in a quartz cuvette, 3ml (0.01 M) aqueous DTAB/SDS/AOT/T-20 was taken and 200 µL (5×10^{-4} M) aqueous MB was added along with 100 µL (0.1M) aqueous $SnCl_2$ (prepared in 1.2 M HC1). To start the catalytic reduction, a fixed volume of the as prepared AgNPs dispersion was added and final volume was made 3.35 mL with Milli-Q water. The final concentration of the AgNPs used in the catalytic MB reduction was 30 µM. The MB color bleaching from blue to colorless was monitored by recording the absorbance at 665 nm. The pH of the reaction solution was ≈ 1.5.

For CR reduction, briefly in a quartz cuvette, 3ml (5×10^{-4} M) aqueous CR was taken and 100 µL (0.2 M) ethanolic $NaBH_4$ was added. To start the catalytic reduction, a known volume of AgNPs dispersion was added and final volume was made 3.2 mL with Milli-Q water, thereby making its final concentration 30 µM. The color bleaching of CR from reddish-orange to colorless was monitored by recording the UV-visible spectra for upto 20 min.

For 4-Nitrophenol reduction, briefly in a quartz cuvette, 3ml (3.5×10^{-4} M) aqueous 4-NP was taken and 100 µL (0.2 M) $NaBH_4$ was added. To start the catalytic reduction, a known volume of AgNPs dispersion was added and final volume was made 3.2 mL with Milli-Q water, thereby making its final concentration 30 µM. The color change of 4-Nitrophenol from bright yellow to colorless was monitored by recording the UV-visible spectra for upto 1 h. In all the uncatalyzed reductions, equal volume of water was used in place of aqueous AgNPs. All the reactions were carried out in triplicate.

Result and Discussion

Characterization of f-AgNPs

The peaks at 4.95 and between 4.35-3.14 ppm in ^{1}H NMR of NG (Figure S7) correspond to methylene, hydroxyl, and α, β-methine protons of polysaccharide, amino sugars, proteinaceous amino acid and d-glucopyranosylfuranic acid contents of NG, respectively. The 5.6 and 1.91 ppm peaks infer anomeric proton of sugar and methyl protons, respectively, while peaks ≈5 ppm correspond to the amine protons from amino sugars and proteinaceous NG content. The ^{1}H NMR of AgNP (Figure S8) is similar to that of NG, depicting the presence of polysaccharide, amino sugars, and proteinaceous amino acid from NG at AgNP surface. For Ala-AgNP, a more intense peak at 1.33 ppm (Figure S9) assigned to methyl protons of Ala when compared with the ^{1}H NMR of NG, elucidate functionalization by Ala. The multiple peaks between 7-8 ppm in the ^{1}H NMR of Trp due to the indole group are absent in Trp-AgNP (Figure S10). The disappearance of these peaks infers that the protons responsible for coupling with adjacent protons are now engaged. Possibly, the electron cloud of these protons is hybridized strongly with the functional groups in NG constituents, wherein during Ag^+ ion reduction, the indole group undergoes modification (Figure S10, 7–8 ppm region), and Trp molecules may have polymerized to poly(2,6-indole).[1,2]

In the ^{1}H NMR of Met-AgNP (Figure S11), peaks at 2.19 and 2.67 ppm corresponding to methyl and methylene protons (-S-C) of Met, respectively, have shifted upfield when compared to Met (Figure S11, 1.98 and 2.49 ppm). For Met-AgNP, the methine proton (-S-C) peak at 3.72 ppm is more intense than for NG and AgNP, illustrating functionalization by Met. The peaks at 7.07 and 7.89 ppm in the ^{1}H NMR of His-AgNP (Figure S12) infers aromatic protons of imidazole group, which have shifted downfield when compared to His (Figure S12, 6.88 and 7.58 ppm), elucidating functionalization by His. In the ^{1}H NMR of Glu-AgNP (Figure S13), peaks at 1.98 and 2.26 ppm are assigned to methylene protons, whereas peak at 3.61 is assigned to methine

proton of Glu. For Glu-AgNP, peak at 2.40 ppm (protons coordinated to the α-carbon of the Glu) shifted upfield to 2.26 ppm, while the intensity of the peak at 3.61 ppm became more intense than in NG (Figure S13), illustrating functionalization by Glu. The peaks between 2.67 and 2.82 ppm in the ^{1}H NMR of Asp-AgNP (Figure S14) correspond to methylene protons of Asp. No peak shifting observed for Asp-AgNP when compared to Asp suggests similar functional activities by Asp. The peaks at 4.95 and between 4.35-3.14 ppm in the ^{1}H NMR of AgNP and f-AgNPs further confirmed their capping with polysaccharides and proteins of NG.

Table S1. The d-Spacing Values and Crystallite Size of Ag_2O and Ag Crystallites Present in AgNPs: AgNP, Ala-AgNP, Trp-AgNP, Met-AgNP, His-AgNP, Glu-AgNP, and Asp-AgNP; calculated using Debye–Scherrer equation

2θ	Plane	d-spacing (Standard)[3,4]	d-spacing (observed)	Size (nm)
		AgNP		
		Ag_2O		
28.1	110	0.33658	0.33726	123
32.5	111	0.27482	0.27562	45
46.4	211	0.19433	0.19588	129
54.9	220	0.16829	0.16721	30
57.5	309	N/A	0.16023	39
67.5	222	0.13741	0.13885	36
		Ag		
38.4	111	0.23480	0.23422	18
		Ala-AgNP		
		Ag_2O		
28.0	110	0.33658	0.33651	54
32.4	111	0.27482	0.27644	62
46.3	211	0.19433	0.19591	74
54.9	220	0.16829	0.16735	54
57.5	309	N/A	0.16027	45
67.4	222	0.13741	0.13894	57
		Ag		
38.5	111	0.23480	0.23398	18
44.6	200	0.20300	0.20309	11
64.8	220	0.14370	0.14394	14
		Trp-AgNP		
		Ag_2O		
27.9	110	0.33658	0.33644	54
32.3	111	0.27482	0.27691	41
46.1	211	0.19433	0.19697	26
54.7	220	0.16829	0.16790	33
57.3	309	N/A	0.16073	23
		Ag		
38.5	111	0.23480	0.23382	13
44.3	200	0.20300	0.20450	11
64.8	220	0.14370	0.14392	12
77.7	311	0.12290	0.12291	17
		Met-AgNP		
		Ag_2O		
28.1	110	0.33658	0.33776	35
32.6	111	0.27482	0.27509	35
46.6	211	0.19433	0.19505	74
55.1	220	0.16829	0.16681	54
57.7	309	N/A	0.15986	30
67.7	222	0.13741	0.13849	24

		Ag		
38.6	111	0.23480	0.23335	10
65.0	220	0.14370	0.14349	18
		His-AgNP		
		Ag_2O		
28.2	110	0.33658	0.33684	61
32.5	111	0.27482	0.27541	28
46.5	211	0.19433	0.19546	32
55.1	220	0.16829	0.16674	11
57.7	309	N/A	0.15987	23
		Ag		
38.5	111	0.23480	0.23399	14
44.5	200	0.20300	0.20358	8
64.8	220	0.14370	0.14379	14
78.0	311	0.12290	0.12255	15
81.9	222	0.11750	0.11752	6
		Glu-AgNP		
		Ag_2O		
28.0	110	0.33658	0.33691	61
32.3	111	0.27482	0.27683	49
46.3	211	0.19433	0.19623	129
54.8	220	0.16829	0.16751	45
57.4	309	N/A	0.16049	30
67.4	222	0.13741	0.13898	36
		Ag		
38.4	111	0.23480	0.23433	11
64.8	220	0.14370	0.14393	12
77.6	311	0.12290	0.12300	19
		Asp-AgNP		
		Ag_2O		
28.1	110	0.33658	0.33717	61
32.5	111	0.27482	0.27529	62
46.5	211	0.19433	0.19545	65
55.0	220	0.16829	0.16700	54
57.6	309	N/A	0.15991	77
67.6	222	0.13741	0.13867	71
		Ag		
38.5	111	0.23480	0.23399	18
64.9	220	0.14370	0.14370	23

Table S2. Measured XPS Data from Ag 3d, C 1s, O 1s, and N 1s Spectra

	AgNP	Asp-AgNP	Met-AgNP	His-AgNP	Trp-AgNP	Glu-AgNP	Ala-AgNP
	Binding Energy (eV)						
	366.9	367.5	364	364.4	366.4	367.2	367.3
	368.1	368.9	368.4	368.9	368.2	368.4	368.8
	372.7	373.5	372.6	372.3	372.5	373.1	373.2
Ag 3d	374.1	374.9	374.5	374.9	374.1	374.3	374.7
	281.6	283.3	284.4	285.1	284.9	283.3	284.4
	284.8	285.5		290.5	287.8	286.1	
C 1s		289.1				289.2	
	529.6	531.2	528.1	530.5	530.3	529.8	530.3
	531.5	532.8	529.3	532.4	532	531.5	531.5
			531.4	534.4		532.8	532.7
O 1s			532.3				
	398.8	399.2	399	396.6	397.1	399.6	398.6
			400.1	399.1	399.5	401	
N 1s					402.4		

Table S3. Percentage of Ag^0 and Ag_2O Content in AgNPs Calculated from XPS Analysis and UV-visible Absorbance Spectra

AgNPs	(%) Ag^0 from XPS	(%) Ag_2O from XPS	(%) Ag^0 from Absorbance spectra	(%) Ag_2O from Absorbance spectra
AgNP	33.53	66.47	36.33	63.67
Ala-AgNP	37.52	62.48	41.03	58.97
Trp-AgNP	76.84	23.16	85.68	14.32
Met-AgNP	71.36	28.64	79.08	20.92
His-AgNP	73.89	26.11	84.58	15.42
Glu-AgNP	59.09	40.91	65.97	34.03
Asp-AgNP	38.87	61.13	45.74	54.26

Table S4. Summary of the Amount of MB, Amount of Reducing Agent and Amount of Catalyst Used in MB Reduction from Literature

Catalyst	Amount of MB (mg)	Amount of reducing agent (μmol)	Amount of catalyst used	MB removal (%)	Time	Refs
Au–CNx composite	0.030	visible light	1 mg	96%	120 min	5
TiO_2 (P25)-graphene	0.345	UV	30 mg	70-85%	55 min	6
AuNP	0.500	400 μmol $NaBH_4$	1 mg	100%	8 min	7
AgNP	0.300	158.6 μmol $NaBH_4$	-	100%	8-20 min	8
AuNP	0.330	211.5 μmol $NaBH_4$	-	100%	4-12 min	8
AgNP	0.320	100 μmol $NaBH_4$	≈ 0.07 mg	100%	8-19 min	9
AgNP	0.320	845.5 μmol $NaBH_4$	≈ 0.07 mg	100%	8-12 min	10
Ag–In–Ni–S	3.199	sunlight	20 mg	100%	2 min	11
AgNP	0.480	10 μmol $NaBH_4$	11 mg	100%	15 min	12
AuNP	0.008	10 μmol $SnCl_2$	0.065 mg	100%	10-35 min	13
p(TA)–Cu ILs composite	10.235	1982.6 μmol $NaBH_4$	0.0039 mmol	100%	3 min	14
GT-Fe NPs	2.303	5.0 mL 10.0% H_2O_2	50.0 mg	≈50%	5 min	15
Ni NS	0.026	0.04 μmol $NaBH_4$	0.2 mg	100%	40 sec	16
Cu_2O@Ag	0.058	6 μmol $NaBH_4$	0.1 mg	80%	5-9 min	17
AgNPs-Fe_3O_4@PDA	0.150	50 μmol $NaBH_4$	5 mg	100%	30 min	18
AgNPs/P(NIPAM-co-DMA) microgels	0.015	105.7 μmol $NaBH_4$	0.056 mg	100%	28 min	19
Sacha inchi (SI) oil templated AgNPs	0.050	Sunlight	≈0.022 mg	95%	480 min	20
Graphene oxide (GO)/AgNPs	0.480	10 μmol $NaBH_4$	≈0.054 mg	100%	15 min	21
Ag colloid	0.032	0.75 μmol $NaBH_4$	0.1 mg	65%	10 min	22
Au-PBCGO55	0.010	100 μmol $NaBH_4$	0.003	83%	33 min	23
Ag-PBCGO55	0.010	100 μmol $NaBH_4$	0.003	≈69%	18 min	23
AgDENs	0.001	0.3264 mg H_2O_2	0.15 mL 0.25 μ M	≈70%	150 min	24
AuDENs	0.001	0.3264 mg H_2O_2	0.15 mL 0.25 μ M	≈83%	150 min	24
Fe_3O_4@Tween20@Ag	0.320	10 μmol $NaBH_4$	5 mg	≈93%	17 min	25
AgNPs (in 0.01 M aq. AOT)	0.011	10 μmol $SnCl_2$	0.01 mg	100%	4 min	This work
AgNPs (in 0.01 M aq. SDS)	0.011	10 μmol $SnCl_2$	0.01 mg	100%	4 min	This work
AgNPs (in 0.01 M aq. DTAB)	0.011	10 μmol $SnCl_2$	0.01 mg	100%	5 min	This work
AgNPs (in aq.)	0.011	10 μmol $SnCl_2$	0.01 mg	100%	7 min	This work
Trp-AgNPs (in aq and 0.01 M aq. AOT/SDS/DTAB/T-20))	0.011	10 μmol $SnCl_2$	0.01 mg	100%	40 sec	This work

Table S5. Summary of the Activity Parameter (κ), Dependent on the Rate Constants of the Reaction (k_1) and the Amounts of Catalyst Used for CR Reduction

Catalyst	Amount of catalyst (mg)	k_1 (sec^{-1})	κ ($s^{-1}\cdot g^{-1}$)	Refs
AuNP	1	0.0041	4.1	26
Ag/GO–Chitosan	5	0.0034	0.68	27
Au/GO–Chitosan	5	0.0021	0.428	27
NiS	100	0.0003	0.0029	28
Titanium oxide nanotube arrays	-	0.0002	-	29
CuO nanowires	-	0.0001	-	30
ZnO@CuO nanostructures	-	0.0001	-	30
Fe3O4@CuO nanostructures	-	0.0001	-	30
Ag/GO-G3PAMAM	5	0.0168	3.36	31
Ag/GO-G2PAMAM	5	0.0109	2.18	31
Ag/GO-G1PAMAM	5	0.0048	0.96	31
Au/GO-G3PAMAM	5	0.0121	2.42	31
AgNP	0.011	0.0041	376.67	This work
Ala-AgNP	0.011	0.0025	225.15	This work
Trp-AgNP	0.011	0.0003	23.03	This work
Met-AgNP	0.011	0.0002	22.12	This work
His-AgNP	0.011	0.0020	185.15	This work
Glu-AgNP	0.011	0.0019	176.06	This work
Asp-AgNP	0.011	0.0037	334.85	This work

Table S6. Summary of the Activity Parameter (κ), Dependent on the Rate Constants of the Reaction (k_1) and the Amounts of Catalyst Used for 4-NP Reduction

Catalyst	Amount of catalyst	k_1 (sec^{-1})	κ ($s^{-1}\cdot g^{-1}$)	Refs
AuNPs	3.29	0.0120	3.65	32
Spongy AuNPs	6	0.0021	0.35	33
AuNPs	1.99	0.1699	85.44	34
Au/graphene	0.1	0.0032	31.70	35
Carbon@AuNPs	0.1	0.0054	54.20	36
TAC-Ag-1.0	4	0.0052	1.30	37
TAC-Ag-1.4	5	0.0017	0.41	37
TSC-Ag-1.4	6	0.0004	0.09	37
Ag-NP/C composite	1	0.0017	1.69	38
Fe3O4-@SiO2-Ag	1	0.0077	7.67	39
CNFs@Au	0.1	0.0054	54.20	40
Pd-Au@MWCNT	0.02	0.0018	90.50	41
GO–Chit-AgNPs	5	0.0055	1.10	42
GO–Chit-AuNPs	5	0.0038	0.76	42
SMG-capped AgNPs	0.32	0.0009	2.83	43
glucan-AuNPs	3.5	0.0019	0.54	44
Ala-AgNP	0.011	0.0012	110.45	This work
Met-AgNP	0.011	0.0012	112.27	This work
His-AgNP	0.011	0.0003	25.61	This work
Glu-AgNP	0.011	0.0007	60.15	This work
Asp-AgNP	0.011	0.0009	81.97	This work

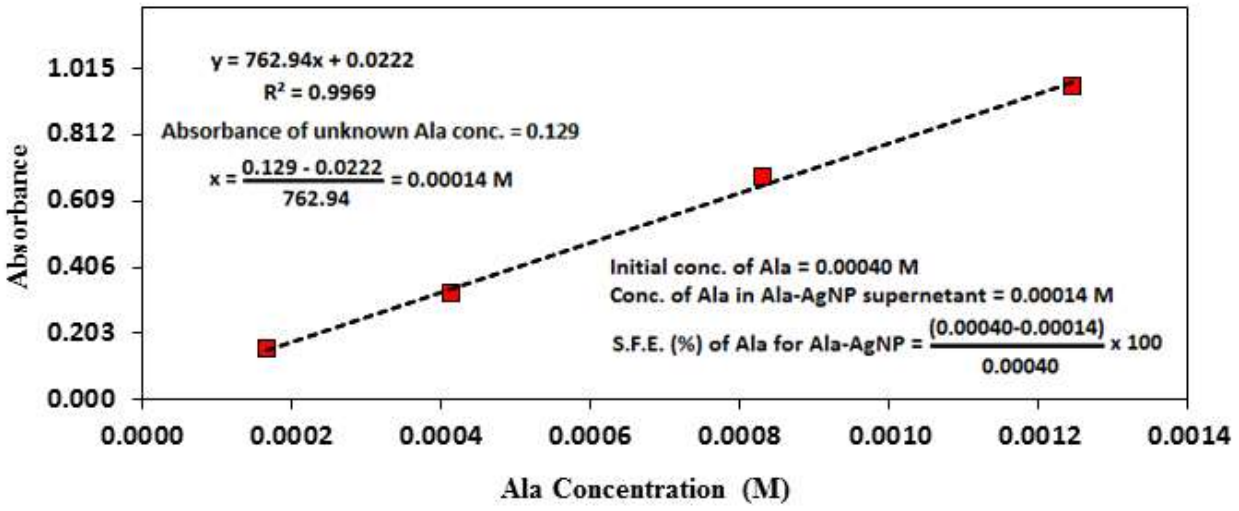

Figure S1. Standard curve of alanine-ninhydrin complex

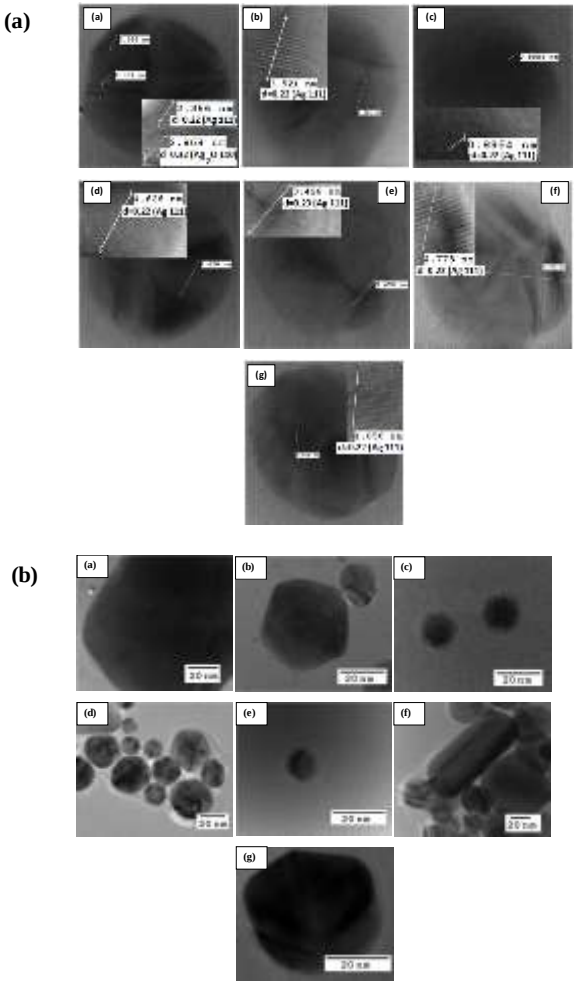

Figure S2. HR-TEM micrograph of (a) AgNP (b) Ala-AgNP (c) Trp-AgNP (d) Met-AgNP (e) His-AgNP (f) Glu-AgNP (g) Asp-AgNP, illustrating capping and lattice spacing of Ag (111)/Ag2O (110) plane

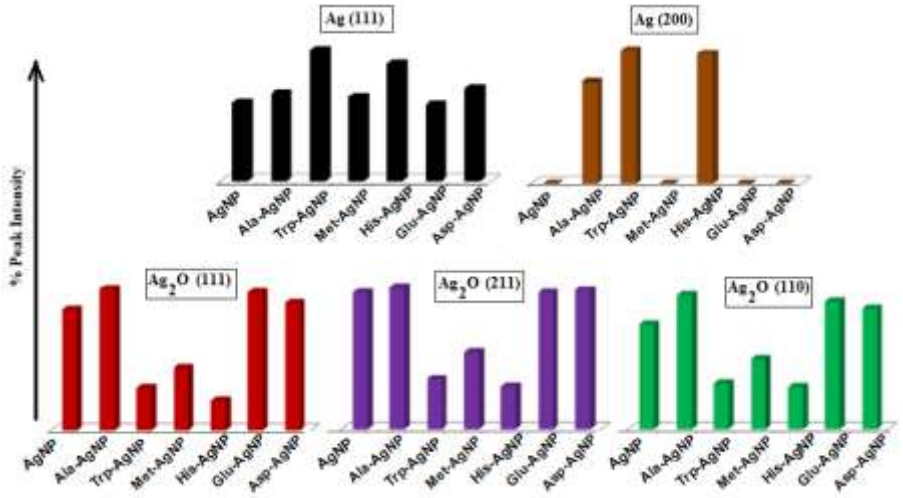

Figure S3. Percentage of XRD peak intensities of various Ag and Ag_2O crystallite lattice planes present in the AgNPs: AgNP, Ala-AgNP, Trp-AgNP, Met-AgNP, His-AgNP, Glu-AgNP, and Asp-AgNP

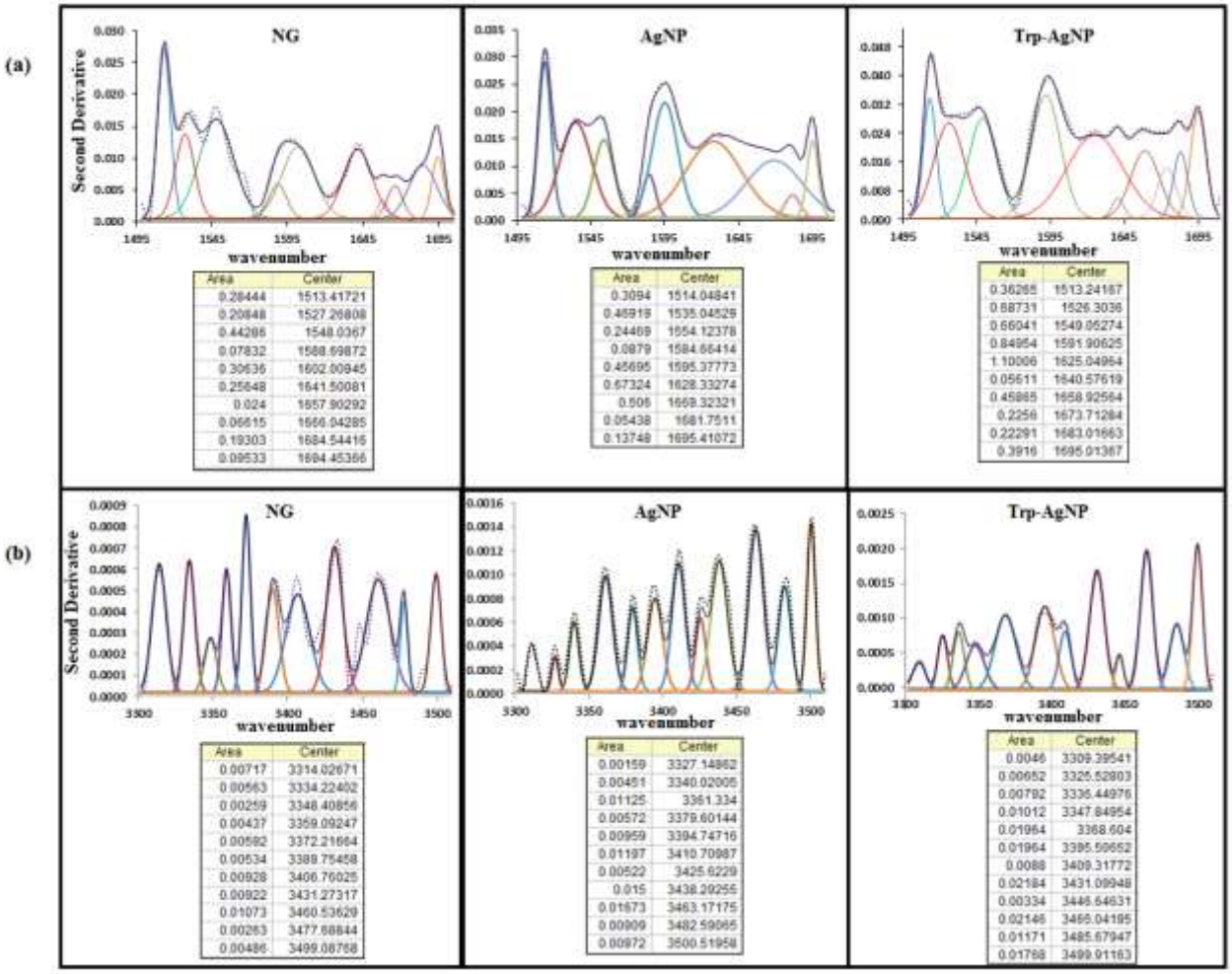

Figure S4. Comparative deconvoluted FTIR spectrums of NG, AgNP and Trp-AgNP at specific wavenumber range (a) 1500-1700 cm^{-1} and (b) 3300-3500 cm^{-1}

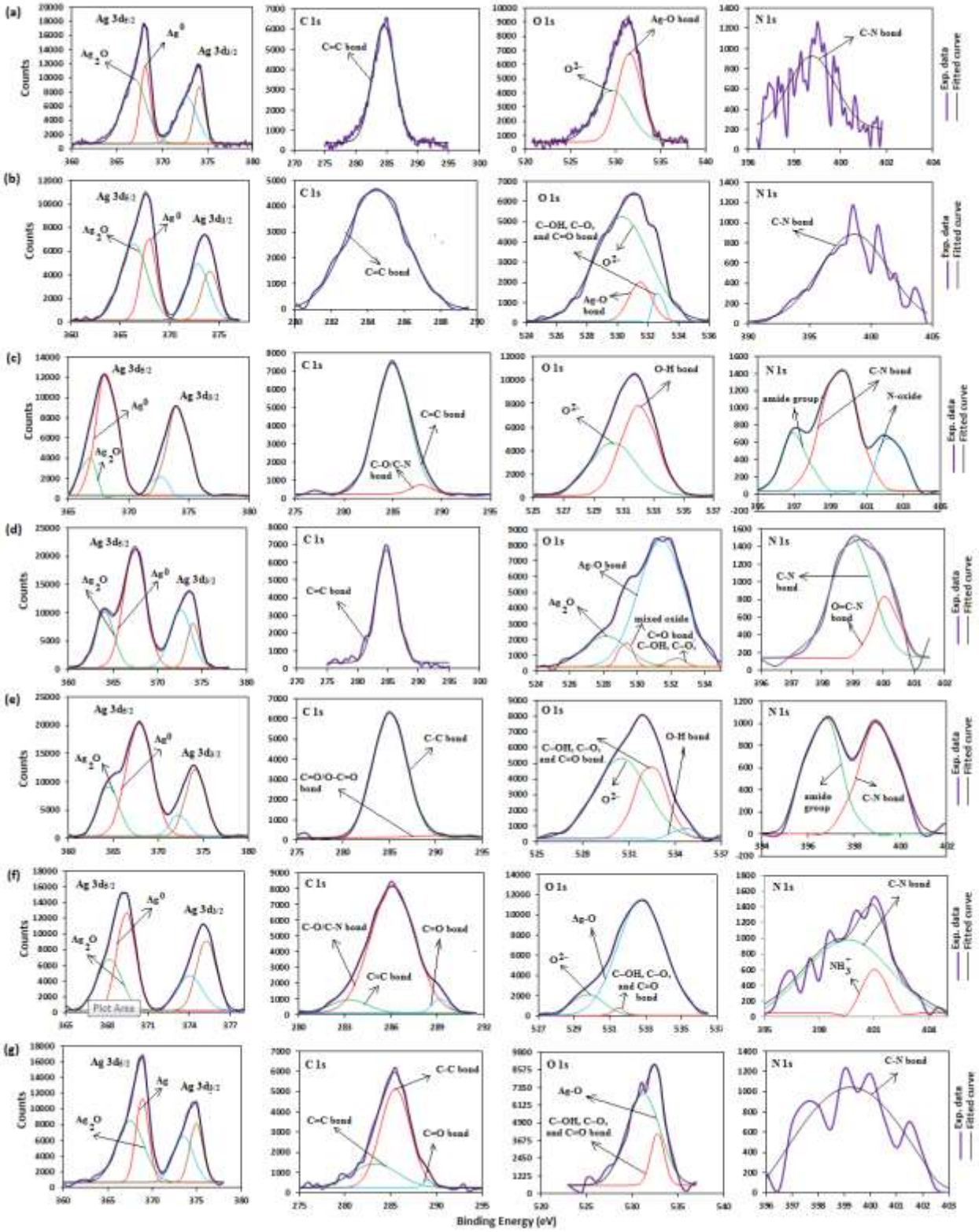

Figure S5. XPS spectral analysis of (a) AgNP (b) Ala-AgNP (c) Trp-AgNP (d) Met-AgNP (e) His-AgNP (f) Glu-AgNP and (g) Asp-AgNP showing corresponding deconvoluted peaks in the high resolution spectra of various elements present, i.e., Ag (3d), O (1s), C (1s), and N (1s)

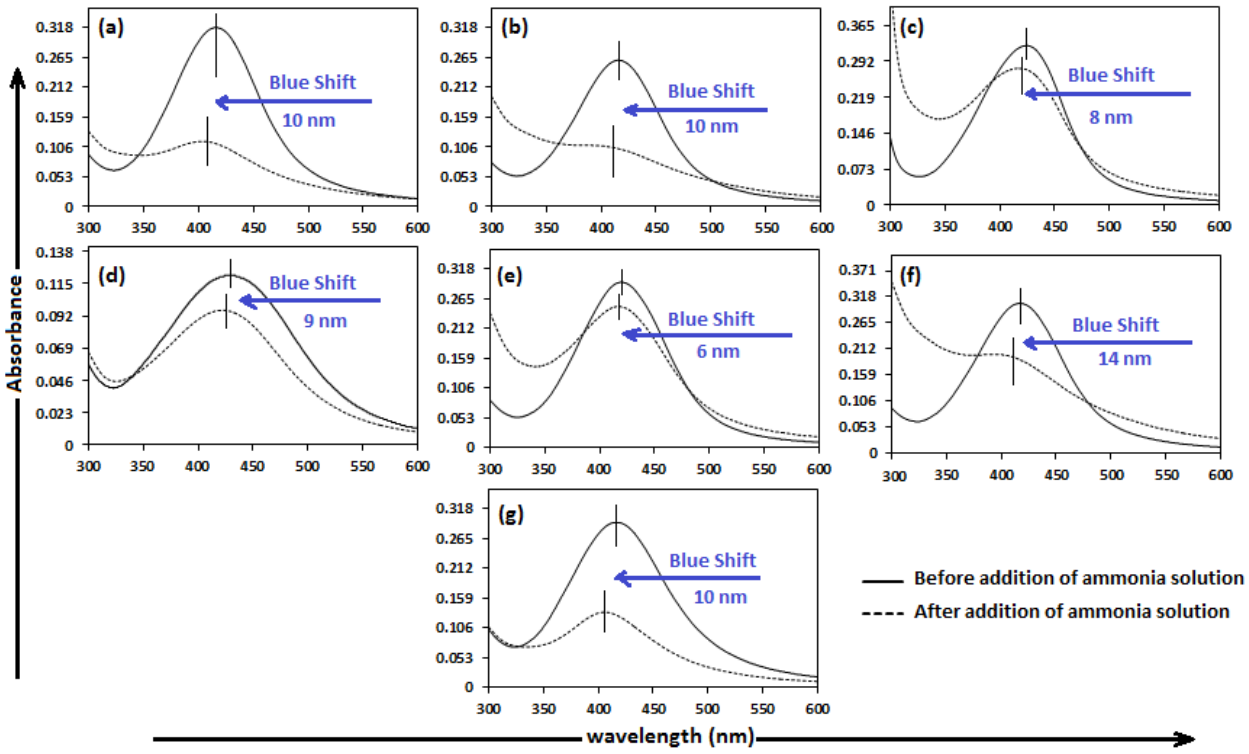

Figure S6. UV-visible absorbance spectra of (a) AgNP (b) Ala-AgNP (c) Trp-AgNP (d) Met-AgNP (e) His-AgNP (f) Glu-AgNP and (g) Asp-AgNP dispersion in absence and presence of aqueous ammonia

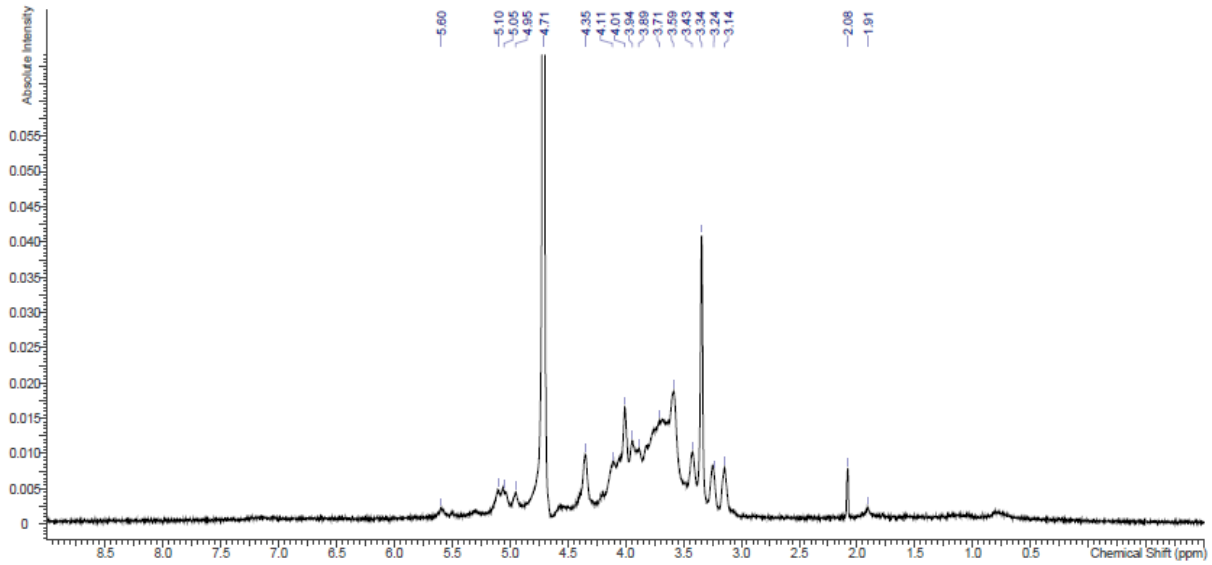

Figure S7. ^{1}H NMR spectrum of NG in D_2O at 500 MHz

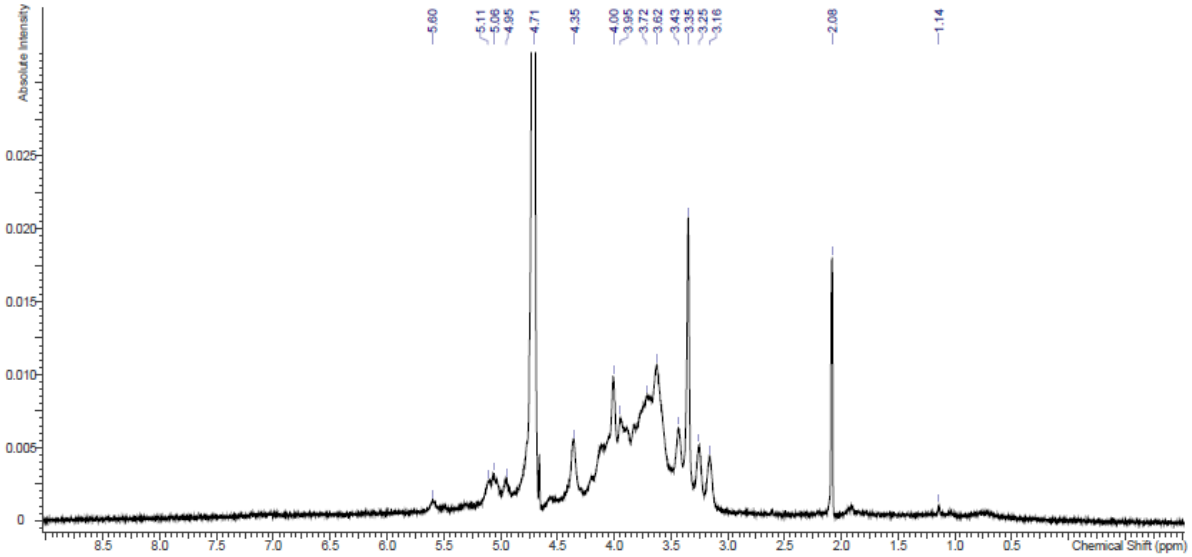

Figure S8. ^{1}H NMR spectrum of AgNP in D_2O at 500 MHz

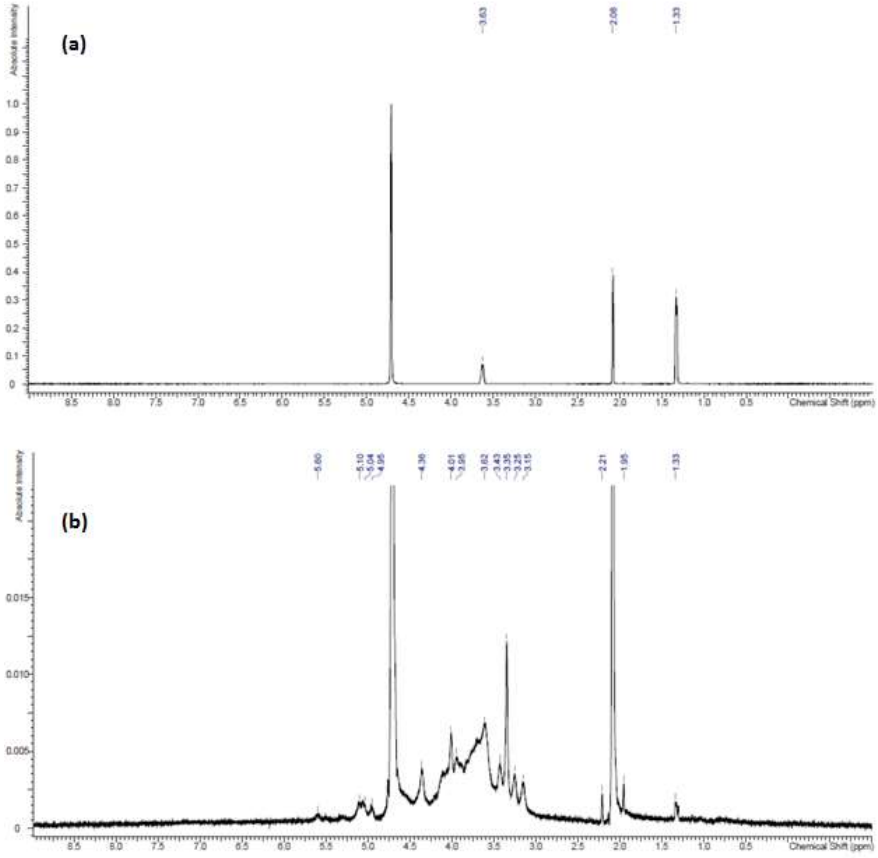

Figure S9. ^{1}H NMR spectrum of (a) Ala and (b) Ala-AgNP in D_2O at 500 MHz

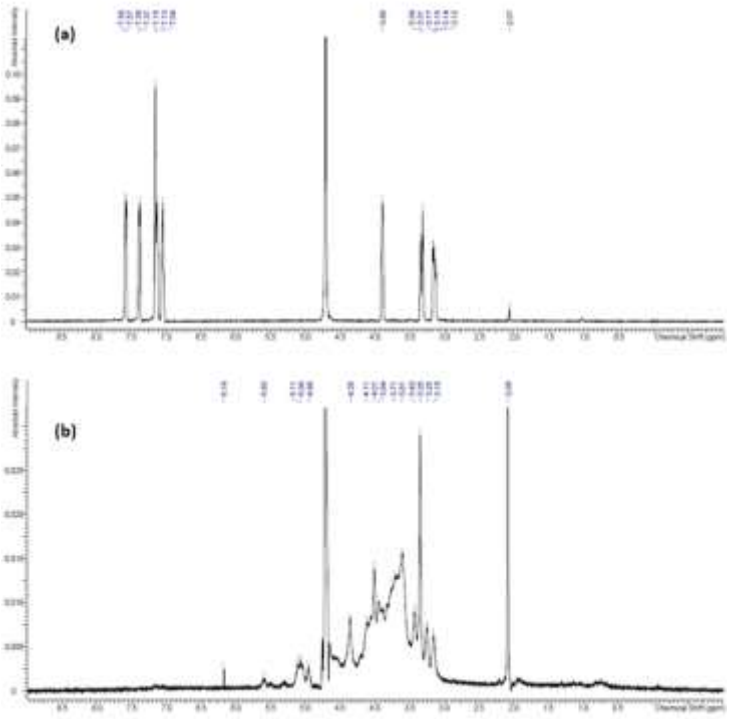

Figure S10. ^{1}H NMR spectrum of (a) Trp and (b) Trp-AgNP in D_2O at 500 MHz

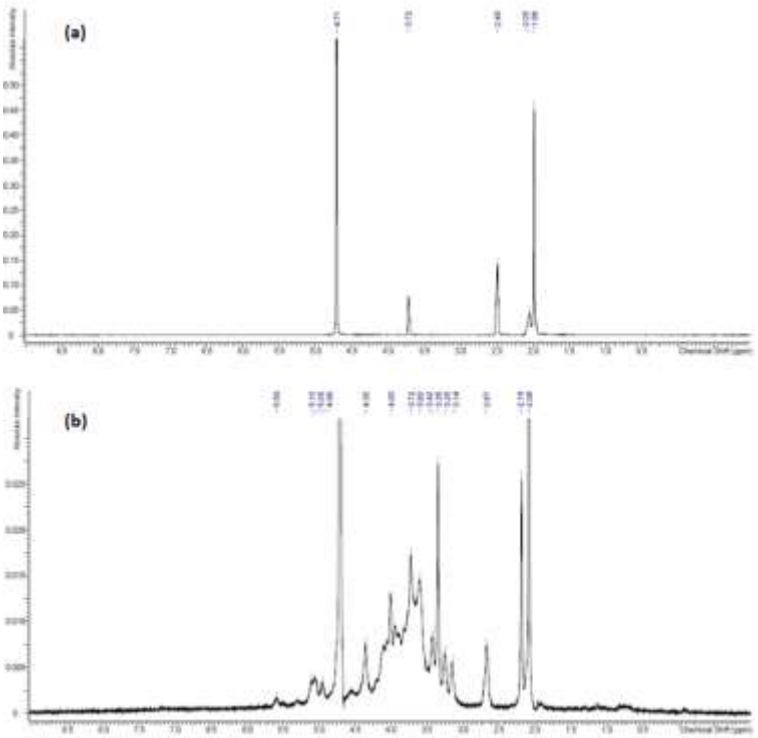

Figure S11. ^{1}H NMR spectrum of (a) Met and (b) Met-AgNP in D_2O at 500 MHz

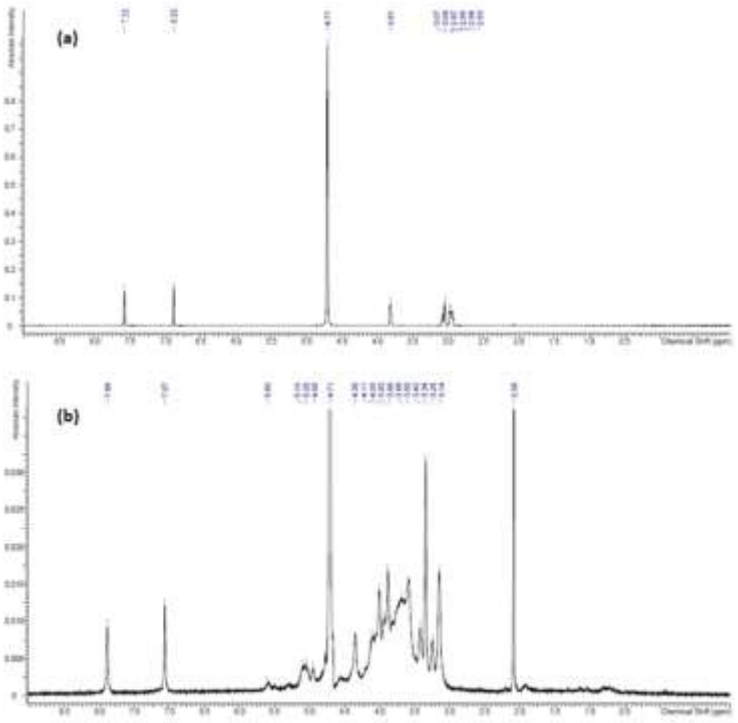

Figure S12. ^{1}H NMR spectrum of (a) His and (b) His-AgNP in D_2O at 500 MHz

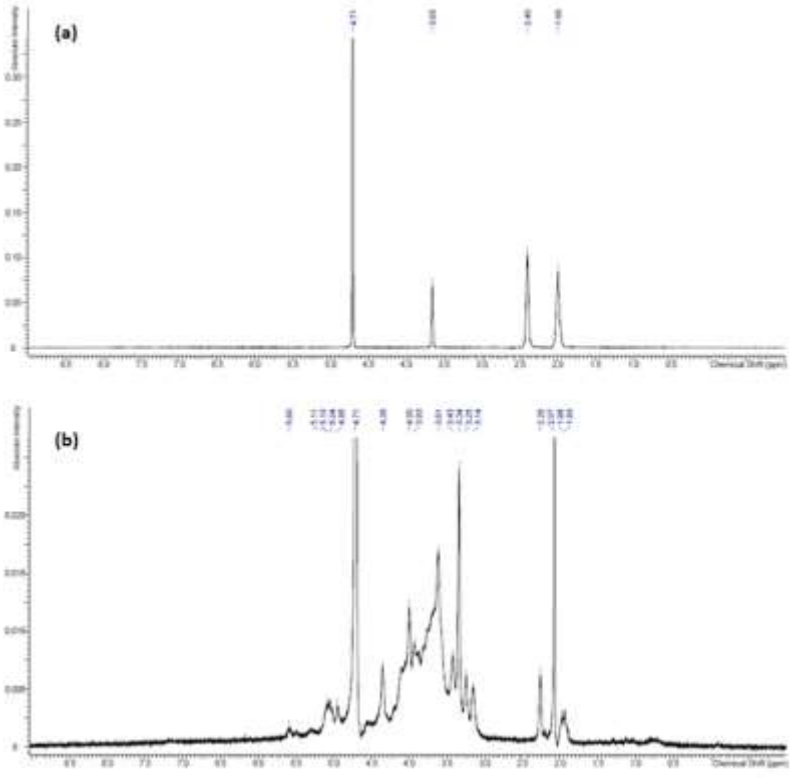

Figure S13. ^{1}H NMR spectrum of (a) Glu and (b) Glu-AgNP in D_2O at 500 MHz

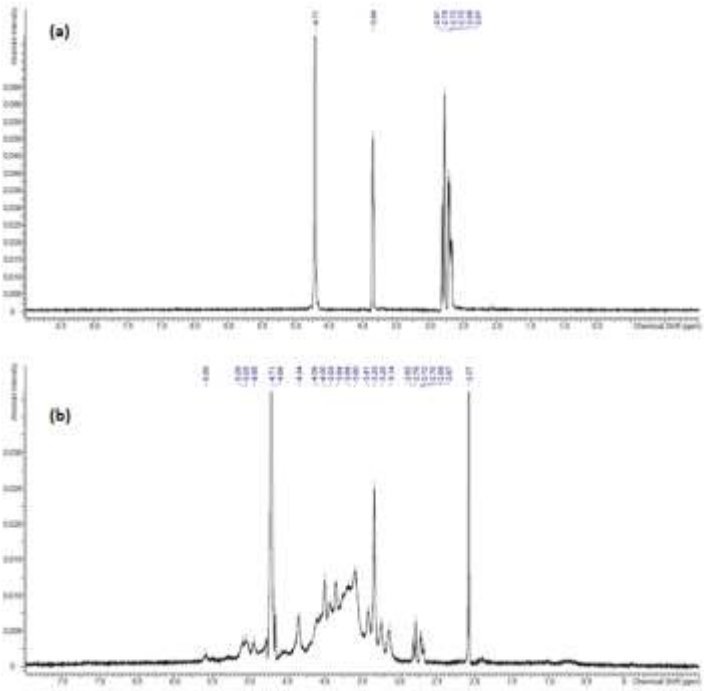

Figure S14. ^{1}H NMR spectrum of (a) Asp and (b) Asp-AgNP in D_2O at 500 MHz

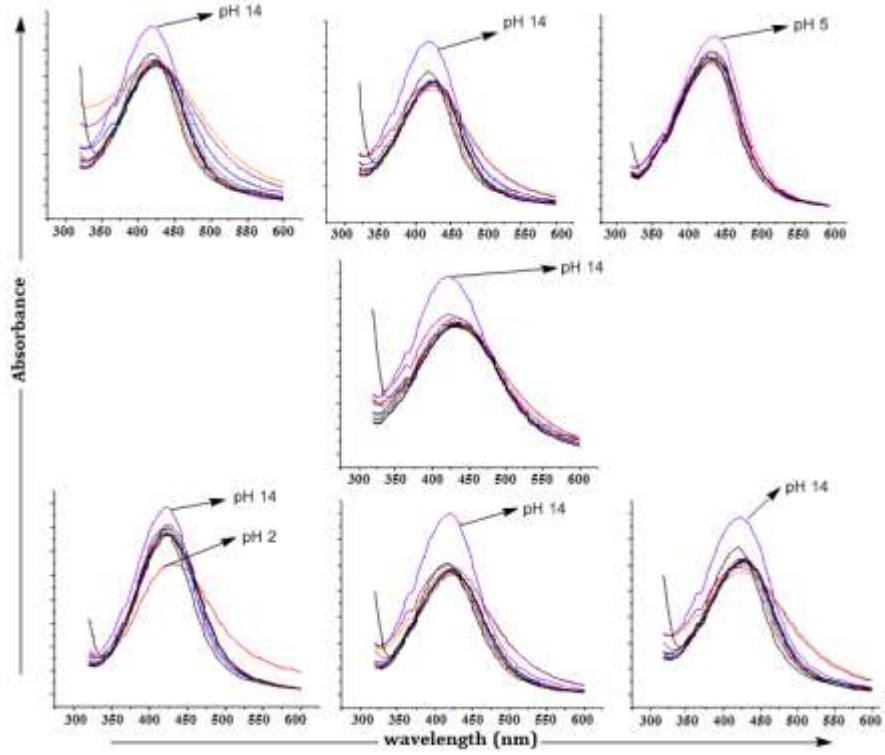

Figure S15. UV-visible absorption spectra of AgNPs: (a) AgNP (b) Ala-AgNP (c) Trp-AgNP (d) Met-AgNP (e) His-AgNP (f) Glu-AgNP (g) Asp-AgNP; in aqueous solutions of pH ranging from 2-14

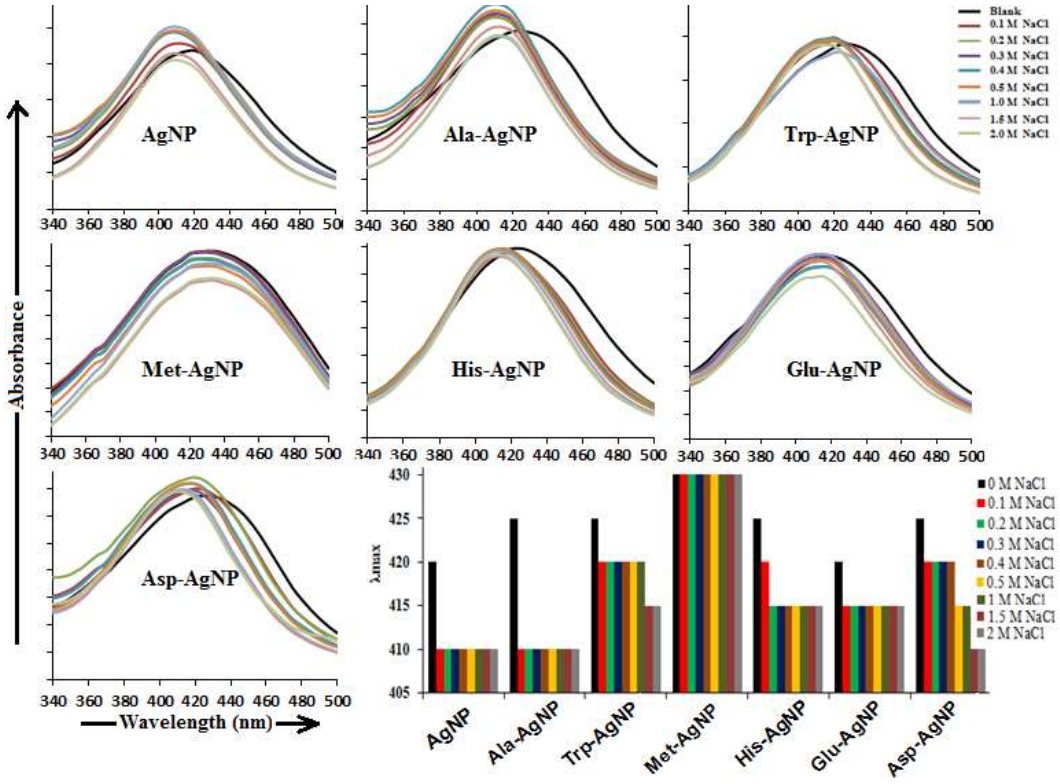

Figure S16. UV-visible absorption spectra of AgNPs in 0–2 M aqueous NaCl

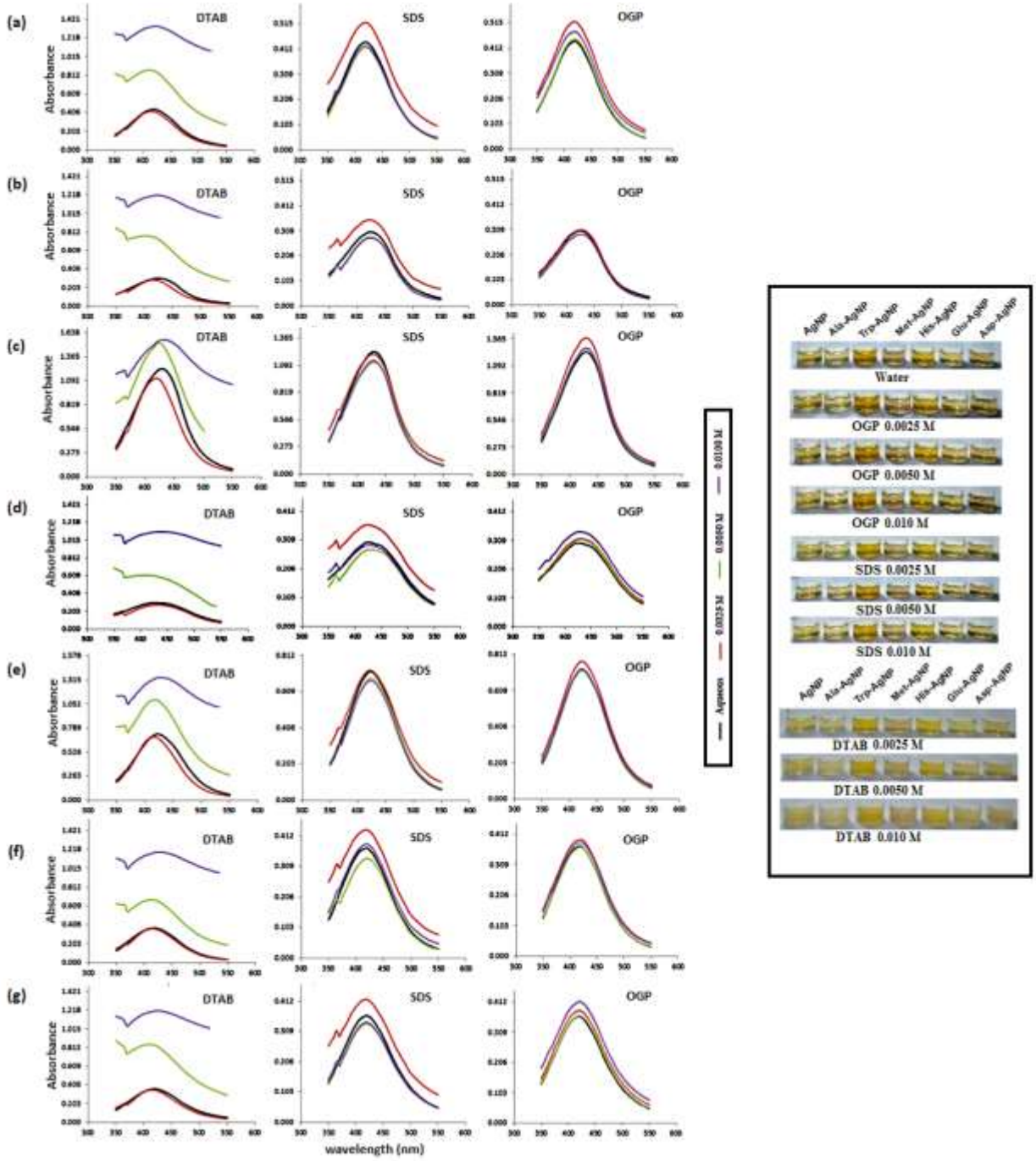

Figure S17. UV-visible spectra of (a) AgNP (b) Ala-AgNP (c) Trp-AgNP (d) Met-AgNP (e) His-AgNP (f) Glu-AgNP (g) Asp-AgNP; in 0.0025–0.010 mol·L^{-1} aqueous surfactants

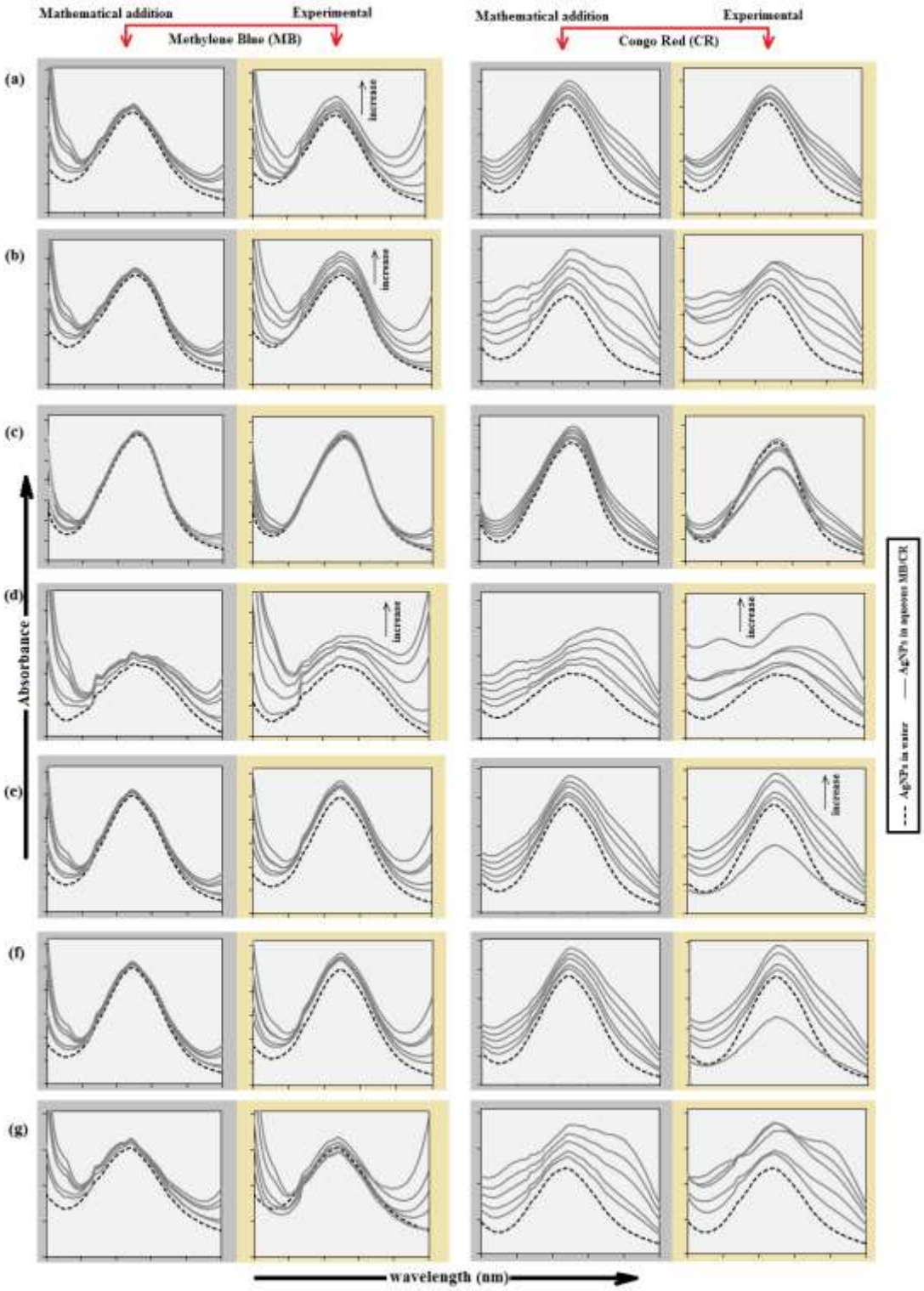

Figure S18. UV-visible spectra of (a) AgNP (b) Ala-AgNP (c) Trp-AgNP (d) Met-AgNP (e) His-AgNP (f) Glu-AgNP (g) Asp-AgNP; in presence of 0-50 μM aqueous MB/CR

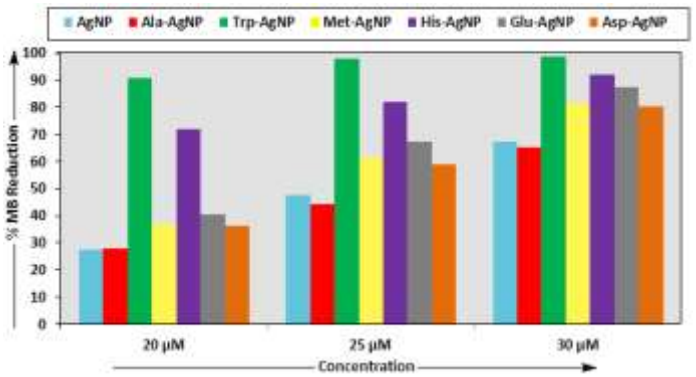

Figure S19. Percentage of MB reduced by acidic $SnCl_2$ after 3 min of catalysis in presence of (20-30 µM) AgNPs: AgNP, Ala-AgNP, Trp-AgNP, Met-AgNP, His-AgNP, Glu-AgNP, and Asp-AgNP; in T-20 micellar medium

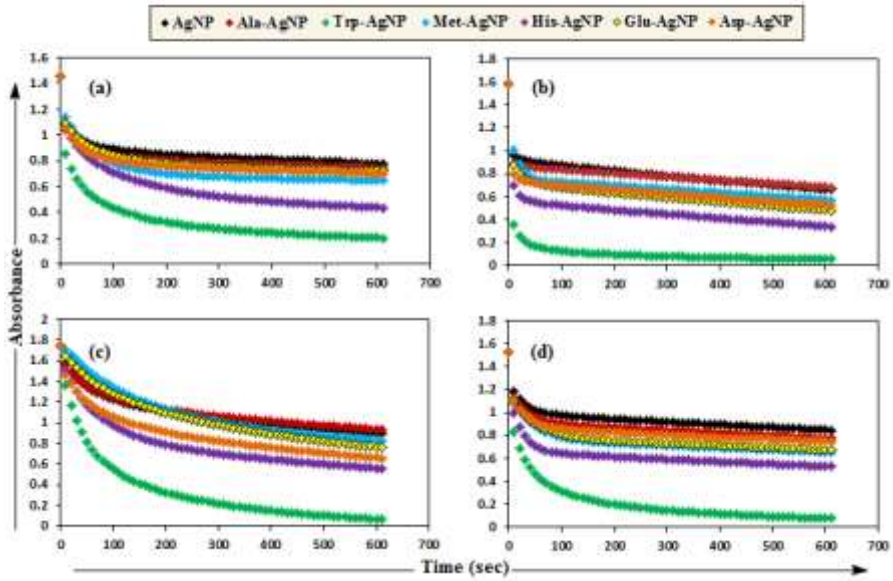

Figure S20. Plot of the absorbance at λ_{max} of MB versus time with 20 µM AgNPs in (a) in 0.01 M aqueous AOT (b) in 0.01 M aqueous SDS (c) in 0.01 M aqueous DTAB (d) in aqueous

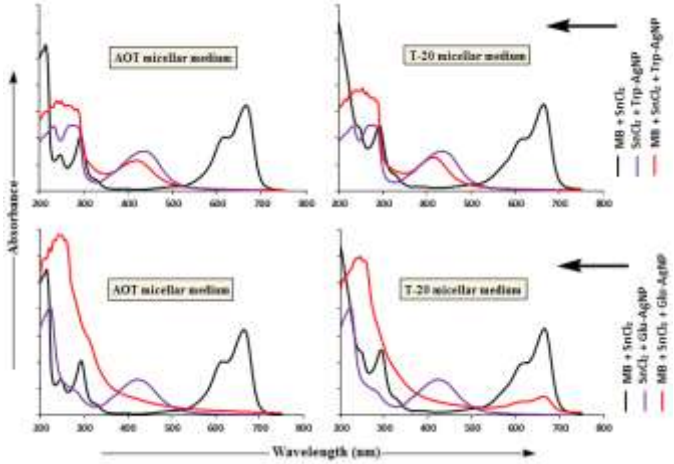

Figure S21. UV-visible absorbance spectra of reaction mixture containing MB and acidic $SnCl_2$ in AOT and T-20 micellar mediums, recorded 20 min after addition of Trp-AgNP and Glu-AgNP

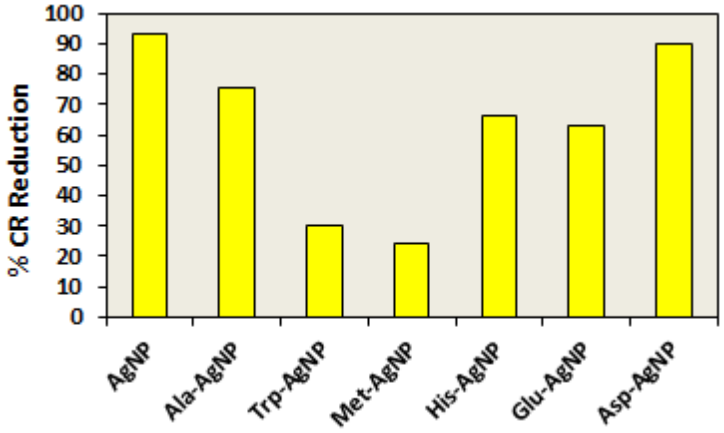

Figure S22. Percentage of CR reduced by $NaBH_4$ after 15 min of catalysis in presence of 30 μM AgNPs: AgNP, Ala-AgNP, Trp-AgNP, Met-AgNP, His-AgNP, Glu-AgNP, and Asp-AgNP

REFERENCES

[1] S. Selvan, *J. Chem. Soc. Chem. Commun.*, 1998, 0, 351-352.

[2] P. Selvakannan, S. Mandal, S. Phadtare, A. Gole, R. Pasricha, S. Adyanthaya and M. Sastry, *J. Colloid Interface Sci.*, 2004, 269, 97–102.

[3] L. Xu, B. Wei, W. Liu, H. Zhang, C. Su and J. Che, *Nanoscale Res. Lett.*, 2013, 8:536.

[4] W. Wei, X. Mao, L. Ortiz and D. Sadoway, *J. Mater. Chem.*, 2011, 21, 432–438.

[5] T. Bhowmik, M.K. Kundu and S. Barman, *RSC Adv*., 2015, 5, 38760–38773.

[6] H. Zhang, X. Lv, Y. Li, Y. Wang and J. Li, *ACS Nano*, 2010, 4(1), 380-386.

[7] B. Paul, B. Bhuyan, D.D. Purkayastha, S. Vadivel and S.S. Dhar, *Mater. Lett.*, 2016, 185, 143-147.

[8] V.S. Suvith and D. Philip, *Spectrochim. Acta Mol. Biomol. Spectrosc.*, 2014, 118, 526–532.

[9] V.K. Vidhu and D. Philip, *Micron*, 2014, 56, 54–62.

[10] V.K. Vidhu and D. Philip, *Micron*, 2014, 117, 102-108.

[11] A. Molla, M. Sahu and S. Hussain, *J. Mater. Chem. A*, 2015, 3, 15616–15625.

[12] M.K. Indana, B.R. Gangapuram, R. Dadigala, R. Bandi, and V. Guttena, *J. of Anal. Sci. Tech.*, 2016, 7:19.

[13] N. Gupta, H.P. Singh and R.K. Sharma, *Colloids Surf., A*, 2010, 367, 102–107.

[14] N. Sahiner, S. Sagbas and N. Aktas, *RSC Adv*., 2015, 5, 18183–18195.

[15] T. Shahwana, S.A. Sirriah, M. Nairat, E. Boyacı, A.E. Eroglu, T.B. Scott and K.R. Hallam, *Chem. Eng. J*., 2011, 172, 258– 266.

[16] N.H. Kalwar, Sirajuddin, R.A. Soomro, S.T.H. Sherazi, K.R. Hallam and A.R. Khaskheli, *International Journal of Metals* 2014, Article ID 126103, 10 pages.

[17] S. Kandula and P. Jeevanandam. *Eur. J. Inorg. Chem*., 2016, 10, 1548–1557.

[18] M. Wu, Y. Li, R. Yue, X. Zhang and Y. Huang, *Scientific Reports*, 2017, 7:42773.

[19] Y. Tang, T. Wu, B. Hu, Q. Yang, L. Liu, B. Yu, Y. Ding and S. Ye, *Mater. Chem. Phy*., 2015, 149–150, 460–466.

[20] B. Kumar, K. Smita, L. Cumbal and A. Debut, *Ind. Crop. Prod*., 2014, 58, 238–243.

[21] T.V.M. Sreekanth, M.J. Jung and I.Y. Eom, *Appl. Sur. Sci*., 2016, 61, 102–106.

[22] C. Wen, M. Shao, S. Zhuo, Z. Lin, and Z. Kang, *Mater. Chem. Phy*., 2012, 135, 780–785.

[23] K.Y. Cho, H.Y. Seo, Y.S. Yeom, P. Kumar, A.S. Lee, K.Y. Baek and H.G. Yoon, *Carbon*, 2016, 105, 340–352.

[24] A.K. Ilunga and R. Meijboom, *J. Mol. Catal. A*, 2016, 411, 48–60.

[25] U. Kurtan, A. Baykal and H. Sözeri, *J. Inorg. Organomet. Polym,*, 2015, 25, 921–929.

[26] B. Paul, B. Bhuyan, D.D. Purkayastha, S. Vadivel and S.S. Dhar, *Mater. Lett*., 2016, 185, 143–147.

[27] R. Rajesh, E. Sujanthi, S.S. Kumar and R. Venkatesan, *Phys. Chem. Chem. Phys*., 2015, 17, 11329-11340.

[28] H. Guo, Y. Ke, D. Wang, K. Lin, R. Shen, J. Chen and W. Weng, *J. Nanopart. Res.*, 2013, 15(3):1475.

[29] T.S. Natarajan, K. Natarajan, H.C. Bajaj and R.J. Tayade, *Ind. Eng. Chem. Res.* **2011**, *50*, 7753–7762.

[30] D. Malwal and P. Gopinath, *Catal. Sci. Technol*., 2016, 6, 4458-4472.

[31] R. Rajesh, S.S. Kumar and R. Venkatesan, *New J. Chem*., 2014, 38, 1551-1558.

[32] M. Rashid and T.K. Mandal, *Adv. Funct. Mater*., 2008, 18, 2261–2271.

[33] M.H. Rashid, R.R. Bhattacharjee, A. Kotal and T.K. Mandal, *Langmuir*, 2006, 22, 7141–7143.

[34] S.K. Das, C. Dickinson, F. Lafir, D.F. Brougham and E. Marsili, *Green Chem*., 2012, 14, 1322–1334.

[35] J. Li, C.Y. Liu and Y Liu, *J. Mater. Chem*., 2012, 22, 8426–8430.

[36] P. Zhang, C.L. Shao, X.H. Li, M.Y. Zhang, X. Zhang, C.Y. Su, N. Lu, K.X. Wang and Y.C. Liu, *Phys. Chem. Chem. Phys*., 2013, 15, 10453–10458.

[37] M.H. Rashid and T.K. Mandal, *J. Phys. Chem. C*, 2007, 111, 16750−16760.

[38] S. Tang, S. Vongehr and X. Meng, *J. Phys. Chem. C*, 2010, 114, 977−982.

[39] Y. Chi, Q. Yuan, Y. Li, J. Tu, L. Zhao, N. Li and X. Li, *J. Colloid Interface Sci*., 2012, 383, 96−102.

[40] P. Zhang, C. Shao, X. Li, M. Zhang, X. Zhang, C. Su, N. Lu, K. Wang and Y. Liu, *Phys. Chem. Chem. Phys*., 2013, 15, 10453–10458.

[41] C.H. Liu, J. Liu, Y.Y. Zhou, X.L. Cai, Y. Lu, X. Gao and S.D. Wang, *Carbon*, 2015, 94, 295–300.

[42] R. Rajesh, E. Sujanthi, S.S. Kumar and R. Venkatesan, *Phys. Chem. Chem. Phys*., 2015, 17, 11329-11340.

[43] M. Krishna, G.B. Reddy, G. Veerabhadram and A. Madhusudhan, *Appl Nanosci*, 2016, 6, 681–689.

[44] I.K. Sen, K. Maity and S.S. Islam, *Carbohydr. Polym*., 2013, 91, 518– 528.